AMERICAN UNIVERSITY OF BEIRUT

Thermal Transport in Si/Ge Nano-Grains using Ab-initio Simulations

by

Alaa Hussein Akkoush

A thesis
submitted in partial fulfillment of the requirements
for the degree of Master of Science
to the Department of Physics
of the Faculty of Arts and Sciences
at the American University of Beirut

Beirut, Lebanon
January 28, 2019

AMERICAN UNIVERSITY OF BEIRUT

Thermal Transport in Si/Ge Nano-Grains using Ab-initio Simulations

by

Alaa Hussein Akkoush

Approved by:

Dr. Michel Kazan Physics		Advisor
Dr. Jihad Touma Physics		Member of Committee
Dr. Leonid Klushin physics		Member of Committee

Date of thesis defense: January 28, 2019

AMERICAN UNIVERSITY OF BEIRUT

THESIS, DISSERTATION, PROJECT RELEASE FORM

Student Name: AKKoush Alaa Hussein
Last First Middle

(X) Master's Thesis ( ) Master's Project ( ) Doctoral Dissertation

☒ I authorize the American University of Beirut to: (a) reproduce hard or electronic copies of my thesis, dissertation, or project; (b) include such copies in the archives and digital repositories of the University; and (c) make freely available such copies to third parties for research or educational purposes.

☐ I authorize the American University of Beirut, to: (a) reproduce hard or electronic copies of it; (b) include such copies in the archives and digital repositories of the University; and (c) make freely available such copies to third parties for research or educational purposes after:

One ___ year from the date of submission of my thesis, dissertation or project.
Two ___ years from the date of submission of my thesis , dissertation or project.
Three ___ years from the date of submission of my thesis , dissertation or project.

Ala Feb, 5 2019
Signature Date

This form is signed when submitting the thesis, dissertation, or project to the University Libraries

Acknowledgements

I would like to acknowledge the ongoing guidance and support that I got from my advisor Dr.Michel Kazan. His door was always open and he was consistently welcoming all my questions and concerns in all aspects of life. This master experience, that lasted two years, I can describe it as a long agonizing delightful journey. From getting used to this new Linux operating system, figuring out how to run the codes, studying the theory behind the codes and their implementation, till deriving a mathematical model for the grains. Not to mention, the failed trails, errors, and calculations that came upon. Besides, I am so grateful that this work opened the doors for me to get where I please to be in my coming Ph.D studies.

I would also like to thank the physics department at the American university of Beirut who gave me this chance in the first place. I enjoyed this experience, especially, the Graduate Assistant-ship they offered me during these two years.

I would like to extend thanks to my committee members Dr.Jihad Touma and Dr.Leonid Klushin. I would like to confess that their courses were the best ones I took at AUB. Dr.Touma's approach in statistical mechanics were unique and extraordinary, whereas, Dr.Klushin's soft matter course was the course that I most worked on, not to mention, how much it substantially improved my computational skills.

I would like to credit the work of this thesis to my brother, whom I remembered I was writing the second chapter of it, while he was in pain. I am thankful and glad his vision was recovered and he is able to see me presenting this work and receiving my masters. Many thanks to my mom and dad, who supported me inspite of our society and its stereotypes.

Thanks to my friends in the Graduate room one by one, they were almost like a family, we spent all day together, studying, eating, discussing and sometimes gossiping.

An Abstract of the Thesis of

Alaa Hussein Akkoush for Master of science
Major: Physics

Title: Thermal Transport in Si/Ge Nano-Grains using Ab-initio Simulations

In this work, we intend to design nano-granular meta-materials in which phonon boundary scattering mechanisms induce strong reduction in the lattice thermal conductivity. Such systems are expected to show high thermoelectric figure of merit and contribute significantly to the efforts done so far to develop alternative energy technologies.

We present a solution for spatial dependent Boltzmann equation within the single mode relaxation time approximation yielding an accurate expression for thermal conductivity of nano-sized materials or nano-grains. Upon using the conservation of heat flux theorem, we develop an expression for thermal conductivity of a monolayer of nano-grains. Then, we use the Diffuse Mismatch Model (DMM) to develop an expression for thermal conductivity of granular materials. The relaxation times are derived from Fermi's golden rule and the harmonic and anharmonic terms of the force constants involved in the model are derived from first principles techniques.

We apply our model to calculate the thermal conductivity of a granular material made up of a mixture of nano-grains of silicon and germanium. The results demonstrate that such a material is characterized by a thermal conductivity as low as the thermal conductivity of SiGe alloy, which is a well-established thermoelectric material for application in environments of very high temperatures. We demonstrate that the mixture of silicon and germanium nano-grains can be more convenient than SiGe alloy in thermoelectric applications, as they do not present the alloys structure stability problems.

Contents

List of Figures

Introduction

Burning fossil fuels raises in our atmosphere the level of carbon dioxide, which is a major contributor to the greenhouse effect and global warming. High-efficiency thermoelectric materials can be a solution for this serious problem. Thermoelectric devices can efficiently convert waste heat into electrical energy and reduce the human dependence on fossil fuel, which may result in a strong reduction in greenhouse emissions.

Over the past decades, there has been enormous interest in thermoelectric materials, driven by the need of fuel-less power generators. This interest in high-efficiency thermoelectric materials is currently increasing with the industrial and military applications, which are generating numerous activities in the field by demanding thermoelectric materials of efficiency higher than those that are currently in use. Our current demand for alternative energy technologies to reduce our dependence on shrinking fossil fuels is also leading to important research activities, including that of high temperature energy harvesting through the direct recovery of waste heat and its conversion into useful electrical energy. Hence, the development of higher performance thermoelectric materials is becoming more and more important. A key factor in developing technologies for high-efficiency energy conversion is the development of higher-performance thermoelectric materials, either completely new or through more ingenious material engineering of existing materials.

The potential of a material in energy conversion is determined in large part by a measure of the materials figure of merit, ZT, which is equal to $\frac{\sigma S^2}{\kappa}$, where S is the Seebeck coefficient, σ is the electrical conductivity, and κ is the thermal conductivity. Some of the research efforts focus on minimizing the thermal conductivity, while other focus on materials that exhibit large power factor(σS^2)[4].

Over the past 30 years, alloys based on Bi_2Te_3 system [$(Bi_{1-x}Sb_x)_2(Te_{1-y}Se_y)_3$] and $Si_{1-y}Ge_y$ system have been extensively studied for their use as thermoelectric materials to perform in a variety of power-generation applications [5]. These traditional thermoelectric materials have undergone extensive investigation, and they appeared to be a little room for future improvement in the common bulk structures. Other high-temperature bulk materials such as skutterudites, clathrates, half-Heusler alloys, and complex chalcogenides have also been investigated. They showed ZT values near 1

due to properties that might be favorable for potential thermoelectric materials. For instance, skutterudites and clathrates are cage-like materials that have voids in which rattler atoms can be inserted to significantly lower the thermal conductivity due to the rattling atoms ability to scatter phonons. Although the thermoelectric figure of merit of these materials has been a practical upper limit for more than 30 years, yet there are no theoretical or thermodynamic reasons for ZT$\approx$1 as an upper limit, and entirely new classes compounds will have to be investigated.

Quantum well systems (0D, 1D, and 2D) take advantage of their low-dimensional character through physical confinements in quantum dots, nanowires, and thin-films structures to enhance the electronic properties of a given material [6][7]. Besides, nanostructured semiconductor materials can scatter mid- to long-wavelength phonon and thereby reduce the lattice thermal conductivity to its minimum[8]. As such, it has been demonstrated that a significant enhancement in ZT occurs through the construction of Bi_2Te_3/Sb_2Te_3 superlattice. These materials exhibited ZT$\approx$ 2.4 at T$\approx$330 K [9]. Furthermore, there have been reports on Si individual nanowires and PbTe/PbTeSe quantum dot structures that yield ZT$\approx$0.6-1.6[10]. This enhancement of the ZT values is due to creating a nanoengineered material that is efficient in thermal insulating while remaining a good electrical conductance. These results confirm the prediction that the best thermoelectric material would behave as a phonon-glass/electron-crystal (PGEC); that is it would have the electrical properties of a crystalline material and thermal properties of an amorphous or glass-like material. It can actually be estimated that an optimized PGEC material could possibly exhibit values of ZT around 4. This gives encouragement that such materials may be possible and could address many of our energy-related problems. A systematic search, subsequent thorough investigation and materials engineering may eventually yield these much-needed materials for the next generation of thermoelectric devices.

In this thesis, we investigate the thermal conductivity of a mixture of nano-grains of Si and Ge, which is a special type of nanostructures. We expect such a system to exhibit an extremely low thermal conductivity, and consequently a high thermoelectric figure of merit, due to an enhanced phonon scattering by the grains boundary. We use first principles techniques to calculate harmonic and anharmonic force constants necessary to solve the linearized Boltzmann transport equation. We account for the contribution of grains boundaries by solving spatial-dependent Boltzmann equation using DFT techniques. One of the key development in that work is that we calculate the thermal conductivity of finite materials (nano-grains) by introducing correction to the thermal conductivity of the bulk counterpart. In that way, the material size enters as a parameter and the calculation of realistic finite materials becomes possible with an affordable simulation time. The interfacial resistance is accounted for by adopting the Diffuse mismatch model DMM [11]with involving the exact dispersion relations of the materials calculated using first principles techniques. We employ the ab-initio open sources AlmaBTE[12] (to compute the thermal conductivity) and SIESTA[13]

(to compute the phonon dispersion curves and related properties in the first Brillouin zone).

0.1 Brief Summary of Chapters

In Chapter 1, density functional theory will be thoroughly discussed, from how it allows us to reach a solvable Schrodinger equation written as density functionals, to how we can find the interatomic force constants we are interested in.

In Chapter 2, two approaches to investigate thermal transport will be discussed; molecular dynamics(MD) and Boltzmann transport equation (BTE). We show that in BTE there are two solution methods known as the relaxation time approximation (RTA) and iterative method. We demonstrate that RTA is widely used though it has limitations as it uses rough approximations, however, Iterative methods relies on force constants calculated from DFT but computationally very expensive.

In chapter 3, we introduce the acoustic mismatch model (AMM) and the diffuse mismatch model (DMM), which are widely used to calculate the boundary thermal resistance. Moreover, DMM is of utmost importance in our system as it present a high density of interfaces.

In chapter 4, we present an analytical model for the thermal resistance at the grain boundaries since thermal boundary resistance is not accounted for in DFT-based calculation with periodic boundary conditions. Then, we present the obtained results and conclude.

0.2 Computational Means

Our computational approach is based on density functional theory (DFT) along with the pseudo-potential approximation [14] . Calculation of Dispersion relations of Silicon and Germanium is carried out using the SIESTA (Spanish Initiative for Electronic Simulations with Thousands of Atoms) electronic structure code [13]. Within the SIESTA code, electronic wave functions are expanded in a basis of Gaussian-type atomic orbitals. We employed the Kleinman-Bylander form of norm-conserving pseudo-potentials. The exchange-correlation energy functional is evaluated using the local Density approximation (LDA) [15]. The energy cutoff is set to 400 Ry throughout the calculations.

The calculation of bulk thermal lattice conductivity of Si and Ge is calculated with the newly established code AlmaBte [16], that solves linearized Boltzman transport

equation using two approaches. The first approach, is the full iterative method[12] after calculating phonons' frequencies from harmonic and anharmonic high order terms in the potential, by applying Density functional theorem [17]. The second method, rely on relaxation time approximation(RTA).

Chapter 1

Density Functional Theory

For a hydrogen atom with a single electron, the Schrodinger equation can be exactly solved. However, for systems with many electrons, the exact Schrodinger equation is very problematic to solve, when taking into account all the possible interactions between all the electrons and the nuclei present in the system. Hence, some approximations for the interaction potentials are applied to find the wave-functions and their corresponding eigenvalues. Density functional theory (DFT) is an approximation method that is utilized to solve the Schrodinger equation for many-body systems[14] without relying on explicit fitting parameters. Yet, it is based on the ground state theory that will be explained through this chapter.

Starting with the non-relativistic time independent Schrodinger equation:

$$\hat{H}\psi_i(r_1, r_2, .., r_N, R_1, R_2, ..., R_M) = E_i\psi_i(r_1, r_2, .., r_N, R_1, R_2, ..., R_M) \tag{1.1}$$

where $\hat{H}$, ψ, and E are the Hamiltonian energy operator, wavefunction, and the total energy of the system respectively, for N electrons and M nuclei. Equation (1.1) can also be written as:

$$\begin{aligned}\hat{H} = -\frac{1}{2}\sum_{i=1}^{N}\frac{1}{m_i}\nabla_i^2 - \frac{1}{2}\sum_{A=1}^{M}\frac{1}{M_A}\nabla_A^2 - \sum_{i=1}^{N}\sum_{A=1}^{M}\frac{Z_A}{r_{iA}} \\ + \sum_{i=1}^{N}\sum_{j>i}^{N}\frac{1}{r_{ij}} + \sum_{A=1}^{M}\sum_{B>A}^{M}\frac{Z_A Z_B}{R_{AB}}\end{aligned} \tag{1.2}$$

with $\hbar = e^2 = 1$. Here, i and j run over N electrons while A and B denote the M nuclei in the system. The first two terms in Eq.(1.2) describe the kinetic energy of the electrons and the kinetic energy of the nuclei. The third term represents the attractive coulomb interaction between the nuclei and the electrons, the fourth term is the electron-electron interaction while the last term is the nuclear-nuclear interaction. Moreover, m_i is the mass of the electron and M_A the mass of the nucleus. $M_A >>> m_i$, since Eq.(1.2) can be simplified using Born Oppenheimer approximation.

1.1 Born Oppenheimer Approximation

The full wavefunctions cannot be calculated using conventional methods for systems involving many particles. This is because the Schrodinger equation includes $3N_i$ electrons + $3N_A$ nuclei coupled equations. Hence, the first approximation to reduce the complexity, was that proposed by Born and Oppenheimer. The mass of the nucleus is very heavy compared to that of the electrons, i.e, electrons will always see the atoms in a static configuration, thus, the kinetic energy of the nuclei are assumed to be zero and their potential energy is merely a constant. Therefore, the Hamiltonian simplifies to:

$$\hat{H}_{elec} = -\frac{1}{2}\sum_{i=1}^{N}\frac{1}{m_i}\nabla_i^2 - \sum_{i=1}^{N}\sum_{A=1}^{M}\frac{Z_A}{r_{iA}} + \sum_{i=1}^{N}\sum_{j>i}^{N}\frac{1}{r_{ij}} = \hat{T} + \hat{V}_{Ne} + \hat{V}_{ee} \tag{1.3}$$

with $\hat{H}_{elec}$ being the electronic Hamiltonian. Hence,

$$\hat{H}_{elec}\psi_{elec} = E_{elec}\psi_{elec} \tag{1.4}$$

then the total energy is:

$$E_{tot} = E_{elec} + \sum_{A=1}^{M}\sum_{B>A}^{M}\frac{Z_A Z_B}{R_{AB}} \tag{1.5}$$

1.2 Variational Principle

It is a method to find the ground state energy of a system. A ground state wavefunction satisfies the following eigenvalue equation $\hat{H}\psi_0 = E_0\psi_0$ where

$$E_0 \leq \frac{<\psi|\hat{H}|\psi>}{<\psi|\psi>} \tag{1.6}$$

the ground state is found through a finite set of trial functions. To get the ground state wave function ψ_0 and the energy $E[\psi_0] = E_0$, a full minimization to the functional E$[\psi]$ with respect to all allowed N-electrons wave functions is required, i.e,

$$E_0 = min\left\langle\psi|\hat{T} + \hat{V}_{Ne} + \hat{V}_{ee}|\psi\right\rangle \tag{1.7}$$

One of the earliest methods that is based on this scheme is the Hartree-Fock (HF) approximation.

1.3 Hartree-Fock Approximation

In this approximation the ground state wave function is approximated by an anti-symmetric combination of N orthonormal spin orbitals ψ_i using a Slater determinant:

$$\psi_{HF} = \begin{vmatrix} \psi_1(r_1) & \psi_2(r_1) & \dots & \psi_N(r_1) \\ \psi_1(r_2) & \psi_2(r_2) & \dots & \psi_N(r_2) \\ \vdots & \vdots & & \vdots \\ \psi_1(r_N) & \psi_2(r_N) & \dots & \psi_N(r_N) \end{vmatrix} \approx \psi_0 \tag{1.8}$$

In the Hartree-Fock approximation, the orbitals $\psi(r)$ are obtained by minimizing the energy for this determinantal form of ψ_0, i.e,

$$E_{HF} = minE[\psi_{HF}] \tag{1.9}$$

The introduction of the Slater determinant for the wave function and the mean-field approximation made the calculation easier. However, HF is limited to small systems, since it neglects the correlation between electrons. For instance, some noble metals like Au, Cu and Ag have an underestimated cohesive energy by a factor of 3 and some alkali metals are found to be unstable at the level of HF theory [18].
The breakthrough eventually took place when Hohenberg and Kohn presented two theorems [19].

1.4 Hohenberg-Kohn Theorems

Hohenberg and Kohn [19] proved the importance of electron density as a key player in the DFT.

• **The first theorem** states that there is an external potential, as from electrons point of view the interactions with the nuclei is external and this V_{ext} is a unique potential that is determined entirely by the ground-state electron density. Such that, the electron density $\rho(r)$ is defined as the number of electrons per unit volume at a given point r.
In Eq. (1.3): The first term (kinetic energy) and the last term(electron-electron potential) represent the system-independent internal potential, that are independent of the external potential(second term). Hence, a density-dependent internal energy should be there as a universal functional, let us call it $F[\rho]$.

• **The second theorem** states that the electron density that minimizes the energy of the system, using variational principle, is the ground-state electron density ρ_0. Consequently,

$$E_[\rho_0] \leq E[\tilde{\rho}] = T[\tilde{\rho}] + E_{Ne}[\tilde{\rho}] + E_{ee}[\tilde{\rho}] = \int \tilde{\rho}(\vec{r}) V_{Ne}(\vec{r}) d\vec{r} + F[\tilde{\rho}] \tag{1.10}$$

where $\tilde{\rho}$ is the trial electron density that satisfies

$$\tilde{\rho} \geq 0, \quad \int \tilde{\rho}(r) dr = N \quad \text{and} \quad F[\tilde{\rho}] = T[\tilde{\rho}] + E_{ee}[\tilde{\rho}] \tag{1.11}$$

However, $F[\tilde{\rho}]$ does not depend on the external potential, and hence it is a universal functional. Kohn and Sham[20] dealt with the challenge and found an explicit form for $T[\tilde{\rho}]$ and part of $E_{ee}[\tilde{\rho}]$.

1.5 The Kohn-Sham equations

In 1964, Density Functional Theory DFT was initially originated by Kohn and Sham[20]. As written before in Eq.(1.11), the energy linked with a trial electronic density $\tilde{\rho}$ can be given as:

$$E[\tilde{\rho}] = \int \tilde{\rho}(\vec{r}) V_{ext}(\vec{r}) d\vec{r} + F[\tilde{\rho}]$$

and

$$F[\tilde{\rho}] = T[\tilde{\rho}] + E_{ee}[\tilde{\rho}] = T[\tilde{\rho}] + E_H[\tilde{\rho}] + E_Q[\tilde{\rho}]. \tag{1.12}$$

Such that, the electronic interaction energy is separated into the classical Coulomb (Hartree) energy and the exchange-correlation energy. The non-classical part contains the correlation of the electron-electron interaction energy beyond the Hartree term. Hence, E_Q is much like a small correction to the electronic interaction energy E_{ee}.

As mentioned before, we can find the ground state by trying a set of trial densities until we reach a minimum energy for ρ_0. However, this is still computationally unfeasible because of the many-body wavefunction. To solve this problem, Kohn and Sham proposed a conversion from a system of N interacting electrons to a constructed fictitious system of independent electrons. They suggested to use the density of the interacting system and calculate the exact kinetic energy of the non-interacting reference system.

$$T_{KS}[\rho] = \frac{-1}{2} \sum_{i}^{N} < \phi_i | \nabla^2 | \phi_i > \quad \rho_{KS} = \sum_i |\phi_i|^2 \tag{1.13}$$

where the ϕ_i are the orbitals of the non-interacting system, or single-particle wavefunctions . T_{KS} is the kinetic energy of the non-interacting system, and it was accounted by introducing $F[\rho]$ as follows:

$$F[\rho] = T_{KS}[\rho] + E_H[\rho] + E_{xc}[\rho] \tag{1.14}$$

where E_{xc} is known as exchange-correlation energy functional and this functional contains everything that is unknown as depicted in Fig.(1.1). The expression of the exchange-correlation energy functional is of the form:

$$E_{xc} \equiv (T[\rho] - T_{KS}[\rho]) + (E_{ee}[\rho] - E_H[\rho]) \tag{1.15}$$

where T_{KS} is the kinetic energy of an independent electron, and E_H is the Hartree energy defined as :

$$E_H[\rho] = \iint \frac{\rho(r)\rho(r')}{|r - r'|} \, dr \, dr' \tag{1.16}$$

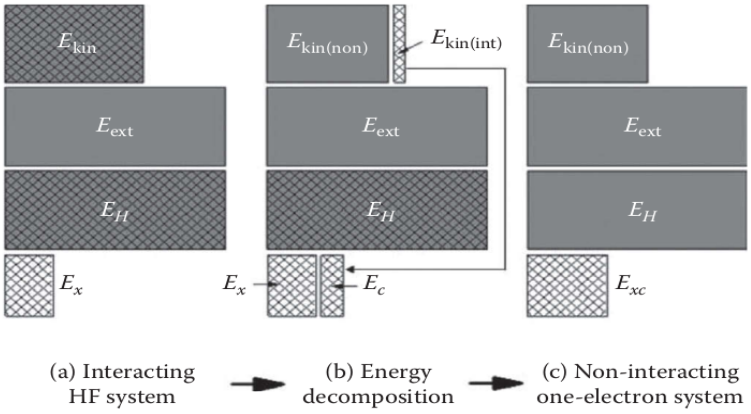

Figure 1.1: Khon-Sham approach, starting from the Hartre-Fock system (a), then decomposing energy (b), and finally the fictitious KS system (the interacting quantum parts are meshed) [1].

A set of self-consistent one-electron equations known as Kohn Sham (KS) equations is obtained after the minimization of the total energy functional by the ground state density, within the constraint that the number of electrons remains fixed. Such that the total electronic energy of the system is found from eigenvalues of these equations.

The Kohn-Sham equations can now be written as an eigenvalue problem as follows:

$$[\frac{-1}{2m}\nabla^2 + V_{ext} + V_H + V_{xc}]\phi_i = \epsilon_i\phi_i \tag{1.17}$$

Then,

$$[\frac{-1}{2m}\nabla^2 + V_{KS}]\phi_i = \epsilon_i\phi_i \tag{1.18}$$

Such that V_{KS} defines the Kohn Sham Hamilton that is defined as a single particle Hamiltonian and it has the form:

$$V_{KS} = V_{ext}(r) + \int \frac{\rho(r')}{|r - r'|}\, dr' + \frac{\delta E_{XC}(\rho)}{\delta\rho(r)} \tag{1.19}$$

V_{KS} depends on the density, then the solution must be acquired self-consistently. The self-consistency condition means that trial electron densities are assumed and can then be used to find the potentials defined in Eq. (1.17). These potentials can then be used to solve the Kohn-Sham equations, resulting in a new density. Self-consistency is achieved when the calculated density equal to the input density as shown in Fig. (1.2). However, the exact form of the exchange-correlation is unknown and attempts to find the optimum form is still in progress. In this thesis we used the simple approximated form of the exchange-correlation, i.e, the local density approximation

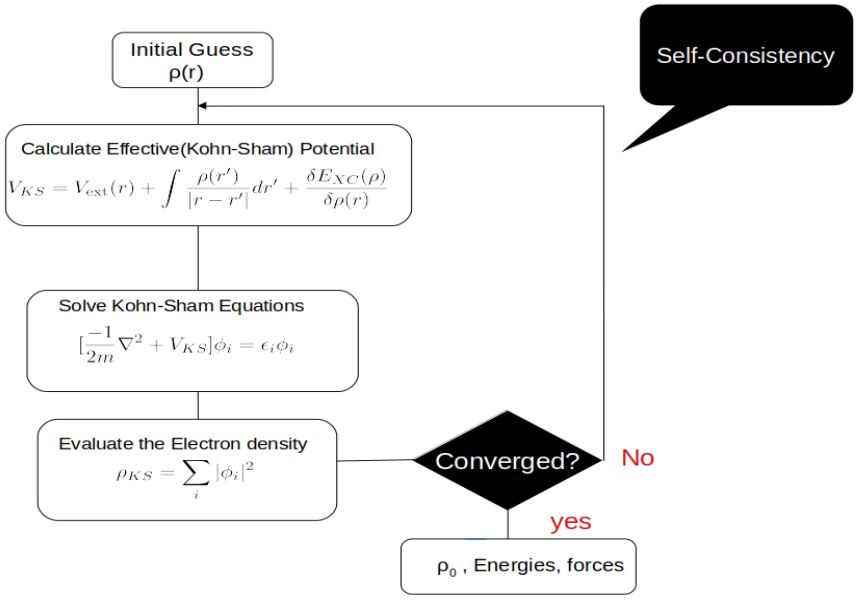

Figure 1.2: Self-consistency in the kohn-sham scheme

(LDA)[21], since we are investigating systems like Si and Ge whose electrons are not highly correlated.

1.6 Local Density Approximation

The local density approximation (LDA) is an approximation to the exchange-correlation functional. The core concept of this approximation is modelling the interaction in the system as that of a uniform electron gas. It can be used when the variation in the electronic density is expected to be slow. LDA assumes that E_{XC} at a point r is of the form:

$$E_{XC}^{LDA} = \int \rho(\vec{r})\epsilon_{XC}(\rho(\vec{r}))d\vec{r} \tag{1.20}$$

where,

$$\rho(\vec{r}) = \sum_i \phi_i$$

and ϵ_{XC} is the exchange-correlation energy per particle, which was originally calculated by Bloch and Dirac in the late 1920's.
However, when LDA overestimates ϵ_{XC} , the first step to go beyond it is to include not only the density at a position r but also its gradient away from r. This approximation is known as the Generalized Gradient Approximation (GGA). However, for elements in group IV and III-V, the phonon dispersion calculated using LDA gives an extremely good agreement with experiments, contrary to GGA[22]. In the case of Si,

unlike GGA, LDA shows a satisfactory agreement with experiments[23]. Hence, the usage of the GGA was unnecessary and all the results in this thesis were performed in the LDA framework.

In order to treat solids in the frame work of DFT, the infinite increase in the number of electrons and the number of atoms in solids should be resolved. Thus, a large number of electrons will be eliminated by the pseudo-potential approach, and a large number of atoms will be eliminated using periodic boundary conditions and the super cell approach.

1.7 Pseudo-potential Approximation

The pseudo-potential (PP) approach was proposed by Heine in 1970 [24], in-which a large number of electrons were eliminated from calculation. The atom is made of core and valence electrons such that the core electrons are frozen with the nucleus, mainly because when the solid is formed the core electrons stay in the potential well generated by the nucleus and the only remaining electrons are the valence ones. In other words, the nuclear charge has much less effect on the valence electrons and is screened by the core electrons; in what we call frozen-core approximation.

In the pseudo-potential approximation the full electron-ion potential is replaced by a weaker pseudo-potential. This potential removes the core electrons and the ionic potential and deals only with the valence electrons. In order to construct the pseudo-potential, we have to take into account the scattering properties of the core electrons and ions with smooth wave-functions that contains correct information about the scattering inside a core radius r_c that is identical to the full potential outside this radius. Such pseudo-potentials are known as "norm-conserving" pseudo-potentials.

As schematically represented in Fig.(1.3), the oscillating wavefunction before r_c is replaced by a soft wave function of the valence electrons and similarly for the potentials with ions. This procedure is specifically termed as pseudization.

After this approximation, the atomic core states are neglected in the self-consistent solution of the KS problem.

$$[\frac{-1}{2m}\nabla^2 + V_{PS}]\phi_i^{PS} = \epsilon_i \phi_i^{PS} \tag{1.21}$$

and

$$\rho(r) = \sum_i \left|\phi_i^{PS}\right|^2 \tag{1.22}$$

For the norm-conserving pseudo-potential, i.e, the pseudo and all electron charge den-

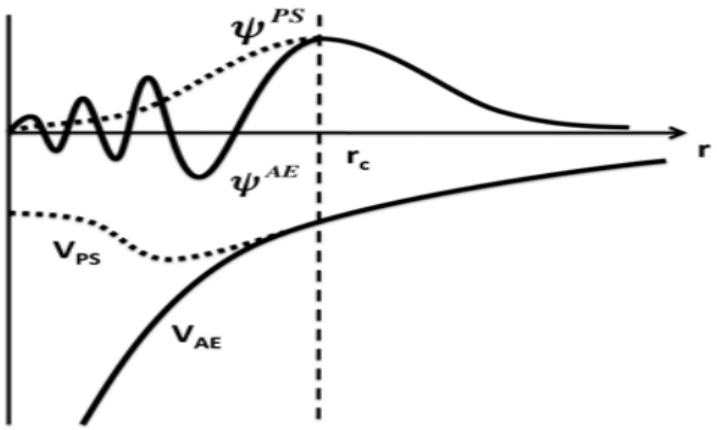

Figure 1.3: Schematic representation of the corresponding pseudo (PS) and all-electron (AE) potentials / wave-functions[2].

sities within the core are constructed to be equal, we have :

$$\int_0^{r_c} \left|\phi_i^{PS}\right|^2 dr = \int_0^{r_c} \left|\phi_i^{AE}\right|^2 \tag{1.23}$$

1.8 Supercell and Periodic Boundary Conditions

To reduce the size of the calculation, several unit cells called supercell is extended to infinity through the periodic boundary condition (PBC). The supercell is then transformed into reciprocal space and fully contained in the first Brillioun zone. Moreover, due to symmetry in rotation and inversion, the first Brillioun zone is further reduced to an irreducible Brillouin zone, without any loss of information. At this stage, Bloch waves can be used to effectively map wave functions with a wave vector k and reciprocal lattice vector G. Selecting as few as possible k-points that are at the same time enough in the IBZ is critical in DFT calculation. Computationally, the k-sampling is done using the Monkhorst-Pack method[25] which creates a grid of k-points evenly spaced throughout the IBZ.

According to Bloch, the wavefunction can be expressed as:

$$\phi_k(\mathbf{r}) = u_k(\mathbf{r}) exp(\mathbf{ik.r})$$

Where $u_k(\mathbf{r})$ is a periodic function, $u_k(\mathbf{r+R}) = u_k(\mathbf{r})$ for **R** being a real lattice vector. Thus, $u_k(\mathbf{r})$ can be written as a Fourier series:

$$u_k(\mathbf{r}) = \sum_G c_k(\mathbf{G}) exp(\mathbf{iG.r})$$

where G is the reciprocal lattice vector. Consequently, the wavefunction becomes:

$$\phi_k(\mathbf{r}) = \sum_G c_k(\mathbf{G}) exp(i\mathbf{(k+G).r})$$

Due to the periodicity of the system in the reciprocal space, the addition or subtraction of a reciprocal lattice vector **G** does not affect neither the wavefunction or the energy. Thus,

$$\Phi_{nk}(\mathbf{r}) = \sum_G c_n(\mathbf{k+G})(r) exp(\mathbf{i(k+G).r})$$

where n is introduced as an additional quantum number, such-that, there are n wave functions for each k-point in a periodic solid.

If we plug the expanded wave function into the KS equations:

$$[\frac{-1}{2}\nabla^2 + V_{KS}] \sum_G c_n(\mathbf{k+G})(r) e^{(\mathbf{i(k+G).r})} = \epsilon_{nk} \sum_G c_n(\mathbf{k+G})(r) e^{(\mathbf{i(k+G).r})}. \quad (1.24)$$

Multiply from the left with exp[i(**k + G) r**] and integrate over the BZ introduces, we get an eigenvalue problem that is easier to solve than the usual KS equation, and can be written as follows:

$$\sum_{G'} \left(\frac{|\mathbf{k+G}|^2}{2} \delta_{GG'} + V_{KS}(\mathbf{G\text{-}G'}) \right) c_n(\mathbf{k + G'}) = \epsilon_{nk} c_n(\mathbf{k + G}) \quad (1.25)$$

where

$$E_{kin} = \frac{\int \phi_{nk} \nabla^2 \phi^*_{nk}}{2} d\mathbf{r} = |\mathbf{k+G}|^2 \frac{\int \phi_{nk} \phi^*_{nk}}{2} d\mathbf{r} = \frac{|\mathbf{k+G}|^2}{2}.$$

Now, by utilizing Bloch theorem and the Fourier series expansion, the computer can handle the above eigenvalue equation. Hence, diagonalizing the vectors $c_n(k, G)$, allows us to calculate ϕ_{nk} and ϵ_{nk}. Then, a new charge density is obtained and a new KS Hamiltonian are calculated, and the process repeats self-consistently until convergence is reached.

It is important to note that to make the size of the expansion of the orbitals finite, we use an energy cut off E_{cut}. Since, we intent to find the lowest ground-state energy, we use the upper energy limit which is the kinetic energy of the free electron calculated previously as $\frac{1}{2}(\mathbf{k+G})^2$.

1.9 Interatomic Force Constants (IFCs)

After finding the equilibrium density of a given atomic configuration, the forces acting on the atoms can be calculated using the Hellmann-Feynman theorem[26]. The

theorem states that, if an exact H and ϕ_i are calculated, the force on an atom is the expectation value of the partial H with respect to atomic position R_I .

$$\mathbf{F} = -\frac{\partial E_{tot}}{\partial \mathbf{R}} = - < \phi_i | \frac{\partial H}{\partial R_I} | \phi_i >$$

This further enables DFT to minimize forces of a given geometry by rearranging the atoms. Hence, to find the equilibrium positions, the forces exerted on the atoms should be minimized. Consequently, a force constant matrix, also known as the Hessian matrix is obtained:

$$\kappa = \frac{\partial E_{tot}(\mathbf{R})}{\partial \mathbf{R}' \partial \mathbf{R}''} = -\frac{\partial \mathbf{F}(\mathbf{R})}{\partial \mathbf{R}''}$$

There are two approaches to calculate the Hessian matrix: linear response theory and frozen phonons approach. The frozen phonon approximation is easy to implement, but has some drawbacks. The Fourier transform of force constant at a wavevector q can be calculated from the variation of forces induced on all the atoms of the supercell by a perturbation. Each atom is displaced in every Cartesian direction along the positive and negative direction. This makes the frozen phonon method extremely unmanageable for large systems.
However, the linear response or the so-called density functional perturbation theory[27] is much faster, which makes the calculation of the anharmonic terms possible. For that reason, it is implemented in most of the ab-initio codes, including **Siesta**[13].

1.9.1 Harmonic IFCs

The second derivative of the electron ground state energy with respect to the atomic displacements represents the reciprocal space harmonic IFCs. We compute the IFCs on a reciprocal space grid because it is computationally more convenient:

$$\phi_{\alpha\beta}^{k,k'}(q, q') = \frac{\partial^2 E_{tot}}{\partial u_\alpha^k(\mathbf{q}) \partial u_\beta^{k'}(\mathbf{q}')}$$

where,

$$u^k(q) = \sum_l u^{lk} exp(i\mathbf{q}\mathbf{R}^l)$$

knowing that R^l is the atomic displacement in the lth unit cell. Applying, newtons law we can obtain the dispersion relation as follows:

$$\sum_{\beta k'} \frac{1}{\sqrt{m_k m_{k'}}} D_{\alpha\beta}^{k,k'}(\mathbf{q}) C_\beta^{k'}(\mathbf{q}) = \omega^2 C_\alpha^{k'}(\mathbf{q})$$

D is called the dynamical matrix, m_k and $m_{k'}$ are the masses of the displaced atoms. Now, phonon frequencies are obtained by diagonalizing the dynamical matrix.

The harmonic IFCs are used to describe the phonon frequencies and eigenvectors. It is where the phonons do not interact with one another. The calculations within the harmonic IFCs has been studied thoroughly and showed supremely good agreement with experimental measurement, for example, phonon dispersion curves. However, the calculation of the third-order anharmonic terms is a tough task.

1.9.2 Anharmonic IFCs

The third-order IFC from which phonon-phonon scattering rates can be obtained is provided from third-order derivatives of the total energy in reciprocal space as:

$$\phi_{\alpha\beta}^{k,k',k''}(q,q',q'') = \frac{\partial^3 E_{tot}}{\partial u_\alpha^k(\mathbf{q})\partial u_\beta^{k'}(\mathbf{q})\partial u_\gamma^{k''}(\mathbf{q}'')}.$$

The calculation of this term was made possible by the Gonze and Vigneron in 1989[28], in which they used "2n+1" theorem of the perturbation theory, that is used for general total energy functionals, constructed from the expectation value of Hamiltonian functional of the electron density like the Kohn-Sham density functional.

Further details will be explained in the next chapter, when phonon scattering mechanisms become more clear.

Chapter 2

Theory of Thermal Transport

In nonmetals, the heat is carried mainly by phonons of mean free paths ranging between 1 and 100 nm. Thermal transport is sufficiently described by Fourier's law of conduction, $Q = -\boldsymbol{\kappa}\boldsymbol{\nabla}\boldsymbol{T}$ where Q is heat flux, κ the thermal conductivity and ∇T the temperature gradient. However, when the size is reduced the properties of semiconductors at these new scales have turned out to be different from those at larger scales. Furthermore, at temperatures above the room temperature, additional phonons processes become significant. For this reason, a significant approach to study phonon transport in solids is the Boltzmann transport equation **BTE** which was originally formulated by Peierls [29]. However, the solution of BTE is non-trivial. In 1958, Callaway proposed an approximation known as relaxation time approximation **RTA**[30]. Later on M.G. Holland developed callaway's model to predict the thermal conductivity of bulk semiconductor materials, by considering additional phonon vibrational behaviors[31]. However, the relaxation time approximation is based on linearising the Boltzmann equation, and it requires parameters that are fitted to experimental data[30]. Recently, molecular dynamics approaches[32] were introduced to calculate the lattice thermal conductivity[33]. Molecular dynamics approach fails at low temperatures, since the behavior of atoms and molecules is described by classical mechanics. Also, molecular dynamics uses forces obtained from semi-empirical force fields. In 2007, Broido[17] presented an ab-initio theoretical approach to describe accurately the phonon thermal transport in semiconductors and insulators without the usage of any fitting parameters. He combined a Boltzmann formalism with density functional theorem **DFT**[34]. DFT enabled him to calculate the harmonic and anharmonic interatomic force constants. Those three approaches are going to be explored in this chapter.

2.1 Molecular Dynamics

Molecular dynamics treatment provide detailed atomic level information about the system under investigation, which is not the case in any other method that uses continuum modelling. In this approach, atoms and molecules follows newton's dynamics such

that the forces are derived from interatomic potentials.

In the following sections, we will discuss the requirements to build a MD simulation, its limitations and determination of the thermal conductivity.

2.1.1 Equations of motion

Atoms are treated as a classical point masses, and the force applied on an atom i is defined as:

$$\mathbf{F}_i = m_i \frac{d^2\mathbf{r}_i}{dt^2} \tag{2.1}$$

Where the forces are calculated from inter-atomic potential, then the force on an atom i due to all its neighbors is written as:

$$\mathbf{F}_i = \sum_{j \neq i} \mathbf{F}_{ij} = -\sum_{j \neq i} \frac{\partial \phi(r_{ij})}{\partial \mathbf{r}_{ij}} \tag{2.2}$$

Knowing that ϕ is an interaction pseudopotential that can be coloumbic, lennard jonnes, etc. There are 6N equations for N atoms without any constraint.

The forces between the atoms are calculated within a MD cell that represents the unit cell of the solid. This unit cell via boundary conditions creates the periodic crystal structure. Nonetheless, we have two types of boundary conditions. First, the atoms are remapped back into the simulation domain when an atom crosses a periodic boundary and not lost. Second, is the periodic boundary conditions. Here, the atoms across the boundaries are interacting. Therefore, periodic boundary conditions mimic bulk structures.

The atoms are allowed to evolve according to the classical equations of motion after initialization the positions and momenta. Once they are set and the system is allowed to evolve, thermal equilibrium has to be reached.

There are two ways to calculate the thermal conductivity:

(1) Non-equilibrium MD (direct method): ΔT is set across the sample and k_l can be computed from Fouriers law.

(2) Equilibrium MD (Green-Kubo method): By determining the equilibrium auto-correlation function for heat current J, thermal conductivity is determined such that it is defined as:

$$k_l = \frac{1}{k_B V T^2} \int_0 < J_x(t) J_x(0) > \tag{2.3}$$

where, V represents the simulation cell volume and $J_x(t)J_x(0)$ are the heat current auto-correlation functions. This integral is replaced by a discrete summation, and Volz et al [35] derived a simpler formula for the auto-correlation function in-terms of time exponential.

A study to predict the thermal transport in Si-Ge random alloys using Stillinger-Weber potential was performed by Skye and Schelling[36]. The predicted thermal conductivity was found to be around an order of magnitude lower than the experiments. Another study was performed to investigate thermal conductivity of Silicon using Tersoff potential and environmental dependent interatomic potential, the results showed either over or underestimate of the thermal conductivity as compared to experiments[17]. Hence, MD simulations qualitatively agree with experiments due to their dependence only on the simple potentials.

2.1.2 Limitations

As previously mentioned, atom are treated as classical point masses, hence, the contribution of the free electrons to the thermal conductivity is not accounted for and the electronic properties of materials cannot be simulated. Furthermore, MD is only applicable in the temperature range where the quantum effects are negligible, i.e, above the Debye temperature of a material, because MD methods rely on classical description of the crystal lattice. Moreover, the length scales involved in MD are of the order of a few hundreds of nanometers. Therefore, there exist computational limitations when it comes to simulating structures such as polycrystalline solids or thick interfaces. The potentials used in MD require a set of parameters determined experimentally. However, the IFCs are generated with a greater accuracy than those obtained from empirical inter-atomic potentials, through ab-initio methods coupled with the linearized Boltzmann equation.

2.2 Boltzmann Transport Equation BTE

Another approach to find the thermal conductivity of the materials is based on solving the Boltzmann transport equation(BTE) for phonons. The interatomic force constants calculated using ab-initio method determine the phonon interactions. From the harmonic terms of the potential (second order interatomic force constants) the phonon frequencies are found, thus, thermal properties such as heat capacity of the material, entropy and free energy can be specified. Moreover, from the third order force constants also calculated from DFT, the an-harmonic scattering is determined. The anharmonic scattering contributes to a major part of the phonon scattering in materials to make the thermal conductivity finite. After calculating the third order force constants from DFT, BTE is solved either iteratively or within the relaxation time approximation(RTA). In 2009, Ward and Broido determined the thermal conductivity for Si and

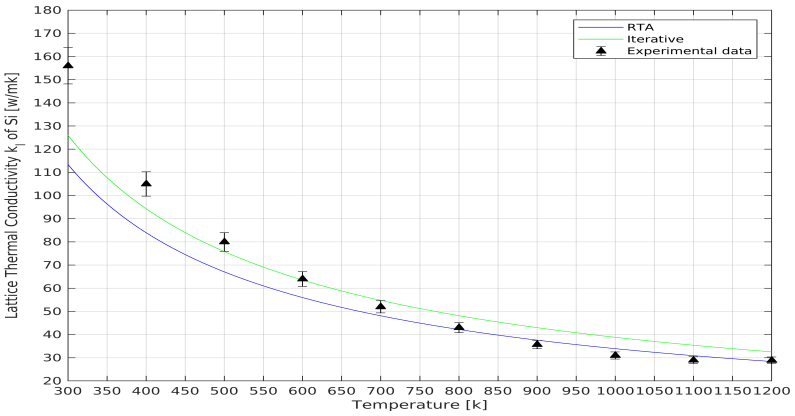

Figure 2.1: Lattice thermal conductivity of Si calculated within RTA and iterative methods compared to experimetal data[3]

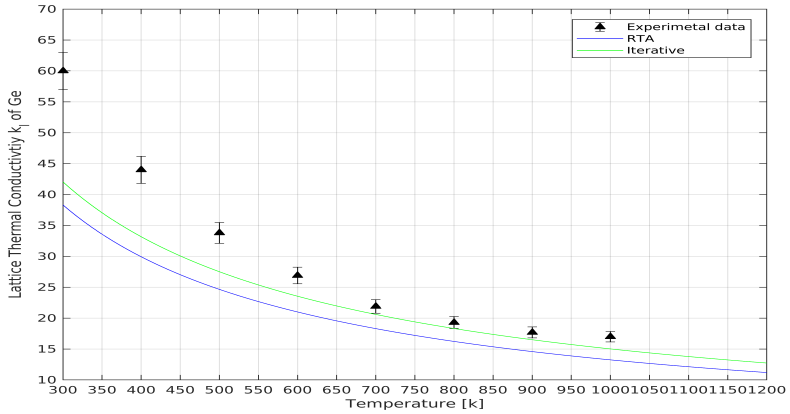

Figure 2.2: Lattice thermal conductivity of Ge calculated within RTA and iterative methods compared to experimental data[3]

Ge by iteratively solving BTE [37]. Their results showed a pretty good agreement with experiments. Furthermore, the lattice thermal conductivity of Si and Ge was calculated within BTE-RTA and found good agreement with the experiments for a large temperature range[38] , as presented in Fig.(2.1 and 2.2).

BTE describes the statistical behaviour of the thermodynamic distribution out of equilibrium. Such that, the evolution of this distribution is due to two mechanisms, one that generates inhomogeneity and the second that tend to restore equilibrium. The former is due to phonons being subjected to diffusion and external fields, while the latter is

due to collisions. The BTE for phonons can thus be written in the form:

$$\frac{\partial N_{kj}}{\partial t}|_{diff} + \frac{\partial N_{kj}}{\partial t}|_{scatt} = \frac{\partial N_{kj}}{\partial t} \tag{2.4}$$

where N_{kj} represents the phonon distribution described by Bose-Einstein distribution function (BE), for a wave vector k and polarization j.

In a steady-state regime the rate of change of N_{kj} with respect to time is zero, since there must be no change in the number of phonons in the crystal, thus,

$$\frac{\partial N_{kj}}{\partial t}|_{diff} + \frac{\partial N_{kj}}{\partial t}|_{scatt} = 0 \tag{2.5}$$

where,

$$\frac{\partial N_{kj}}{\partial t}|_{diff} \equiv \frac{\partial N_{kj}}{\partial t} + \mathbf{v}_k \frac{\partial N_{kj}}{\partial \mathbf{r}} + \mathbf{F}\frac{\partial N_{kj}}{\partial \mathbf{v}} \tag{2.6}$$

Knowing that there is no external force applied(**F=0**) since phonons are quisi-particle and can not be influenced by external forces. And $\mathbf{v}_k$ is the velocity of the mode **k**.

Assuming that the diffusion process is due to temperature gradient ∇T, we can write:

$$\mathbf{v}_k.\boldsymbol{\nabla} T \frac{\partial N_{kj}(k)}{\partial T} = \frac{\partial N_{kj}(k)}{\partial t}|_{scatt} \tag{2.7}$$

The term on the right describes the rate of change of the phonon distribution function due to phonon-phonon scattering, and here lies the complexity of the BTE. Therefore, to have an accurate solution of the phonon BTE, a proper characterization of the microscopic forces and treatment of the inelastic scattering are required.

The potential energy of the lattice is a function of the positions of the nuclei of the atoms that form the solid. At equilibrium the potential energy reaches a minimum. Therefore, any slight displacements of the atoms from equilibrium positions, cause a variation in the potential energy. Accordingly, the potential energy can be expressed as a Taylor series expansion of the energy function in terms of atoms displacements or relative displacements. The first term ϕ_0 of the potential energy represents the equilibrium followed by a quadratic harmonic term in the displacements by the equilibrium conditions. The other terms in the series can be regarded as perturbations on the harmonic term, in which they represent the anharmonic interactions between the vibrational modes. Furthermore, anharmonicity is crucial for the understanding and the modeling of the heat transport.

Therefore, the Taylor series is expressed as:

$$\begin{aligned}\phi = \phi_0 + \sum_{lk\alpha} \phi_\alpha(lk) u_\alpha(lk) + \frac{1}{2}\sum_{lk\alpha}\sum_{l'k'\beta} \phi_{\alpha\beta}(lk, l'k') u_\alpha(lk) u_\beta(l'k') + \\ \frac{1}{3!}\sum_{lk\alpha}\sum_{l'k'\beta}\sum_{l''k''\gamma} \phi_{\alpha\beta\gamma}(lk, l'k', l''k'') u_\alpha(lk) u_\beta(l'k') u_\gamma(l''k'') + ...\end{aligned} \tag{2.8}$$

where l refers to the position of the unit cell and k locates the atom within the unit cell. α, β and γ are the displacement directions in Cartesian coordinates. Also, $u_\alpha(lk)$ is the displacement of the atom k in the unit cell l from their equilibrium positions.

The physical interpretation of $\phi_\alpha(lk)$ is that it is the negative of the force acting on a specific atom in the α direction. In the equilibrium configuration the force vanishes($\phi_{lk} = 0$). $\phi_{\alpha\beta}$ and $\phi_{\alpha\beta\gamma}$ describe the harmonic and the third-order anharmonic interatomic force constants (IFCs) respectively. They can be written as:

$$\phi_{\alpha\beta}(lk, l'k',) = \frac{\partial^2\phi}{\partial u_\alpha(lk)\partial u_\beta(l'k')}|_{\mathbf{u}=0} \tag{2.9}$$

$$\phi_{\alpha\beta\gamma}(lk, l'k', l''k'') = \frac{\partial^3\phi}{\partial u_\alpha(lk)\partial u_\beta(l'k')\partial u_\gamma(l''k'')}|_{\mathbf{u}=0} \tag{2.10}$$

2.2.1 Harmonic interatomic force constants

The equation of motion of the lattice follows immediately:

$$M_k\ddot{u}_\alpha(lk) = -\sum_{l'k'\beta}\phi_{\alpha\beta}(lk, l'k')u_\beta(l'k') \tag{2.11}$$

where M_k is the mass of the k_{th} atom. The coefficient $\phi_{\alpha\beta}(lk, l'k')$ satisfies the symmetry condition :

$$\phi_{\alpha\beta}(lk, l'k') = \phi_{\beta\alpha}(l'k', lk) \tag{2.12}$$

because the partial derivatives can be exchanged. The solution to the equation of motion $u_\alpha(lk)$ can be expressed as follows:

$$u_\alpha(lk) = \frac{1}{\sqrt{M_k}}u_\alpha(k)exp(i(\mathbf{k.x}(l) - wt)) \tag{2.13}$$

Substituting Eq.(2.13) in Eq.(2.11) yields the following matrix:

$$w^2u_\alpha(k) = \sum_{k'\beta}D_{\alpha\beta}(kk'|\mathbf{k})u_\beta(k') \tag{2.14}$$

D(k) is the dynamical matrix in fourier space can be expressed as:

$$D_{\alpha\beta}(kk'|\mathbf{k}) = \frac{1}{\sqrt{M_kM_{k'}}}\sum_{l'}\phi_{\alpha\beta}(lk, l'k')exp(-i\mathbf{k}(\mathbf{x}(l) - \mathbf{x}(l')) \tag{2.15}$$

Consequently, the problem is reduced from solving an infinite set of equations of motion Eq. (2.11) to the problem of solving a set of equations equal to the three times the number of atoms in a unit cell (3N) Eq. (2.15), which in-turn has a nontrivial solution found by the determinantal equation:

$$|D_{\alpha\beta}(kk'|\mathbf{k}) - w^2\delta_{\alpha\beta}\delta_{kk'}| = 0 \tag{2.16}$$

The same result can be derived from the harmonic vibrational Hamiltonian by carrying out the Fourier analysis of the momentum p and the harmonic term in Eq.(2.8), and then introducing raising and lowering operators (a full mathematical proof is found in reference [39]). This method is known as the second quantization method. Then, the known expression for harmonic Hamiltonian is obtained:

$$H^{(2)} = \sum_{\mathbf{k}j} \hbar w_j(\mathbf{k})[a^+_{\mathbf{k}j} a^-_{\mathbf{k}j} + \frac{1}{2}] \tag{2.17}$$

This expression of the harmonic Hamiltonian involves phonon annihilation and creation that is in a diagonal form.

2.2.2 Third order anharmonic interatomic force constants

Following the same mathematical procedure found in ref [39] of coordinate transformation for the anharmonic part of the potential, we obtain:

$$H^{(3)} = \frac{1}{3!} \sum_{\boldsymbol{kk'k''}} \sum_{jj'j''} \delta_{G,\boldsymbol{k}+\boldsymbol{k'}+\boldsymbol{k''}} V^{(3)}(\boldsymbol{kj}, \boldsymbol{k'j'}, \boldsymbol{k''j''}) \tag{2.18}$$

$$\times (a^+_{\mathbf{k}j} - a^-_{\mathbf{k}j})(a^+_{\mathbf{k'}j'} - a^-_{\mathbf{k'}j'})(a^+_{\mathbf{k''}j''} - a^-_{\mathbf{k''}j''})$$

where, $V^{(3)}(\boldsymbol{kj}, \boldsymbol{k'j'}, \boldsymbol{k''j''})$ is the coefficient of the cubic anharmonicity term.

From Eq.(2.17) and Eq.(2.18), we can observe that the harmonic term is diagonal while the anharmonic term is not. This is because anharmonicity carries the properties of phonons who interact with each other and scatter. Those phonons are described as coupled oscillators, whereas harmonicity describes the phonons as independent harmonic oscillators that carry energy and heat.

We get terms like $a^-_{\mathbf{k}j} a^-_{\mathbf{k'}j'} a^+_{\mathbf{k''}j''}$ and $a^-_{\mathbf{k}j} a^+_{\mathbf{k'}j'} a^+_{\mathbf{k''}j''}$ when we expand the parentheses in Eq.(2.18) involving the raising and lowering operators. The terms represent the annihilation of two phonons and the creation of a third phonon of higher energy (see Fig.(2.2)) and annihilation of one phonon and creation of two phonons of lower energy (see Fig.(2.3)) respectively. We neglect other terms because energy must be conserved in all these scattering processes. Hence, the three-phonon scattering processes that satisfy the energy conservation laws will be explored in the following section.

2.2.3 Three-phonon scattering processes

The annihilation of two phonons can be described by the following energy and momentum conservation as:

$$w(\mathbf{k}, j) + w(\mathbf{k'}, j') = w(\mathbf{k''}, j'') \tag{2.19}$$

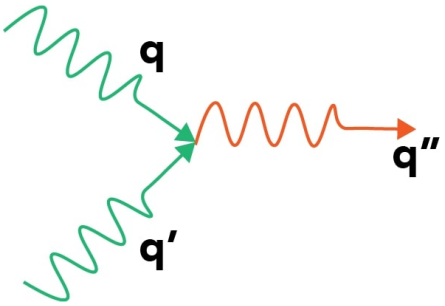

Figure 2.3: annihilation of 2 phonons into 1

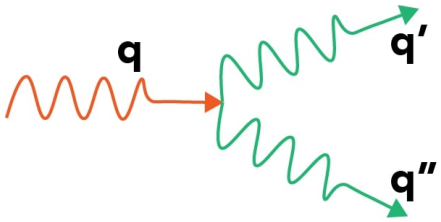

Figure 2.4: annihilation of 1 phonons into 2

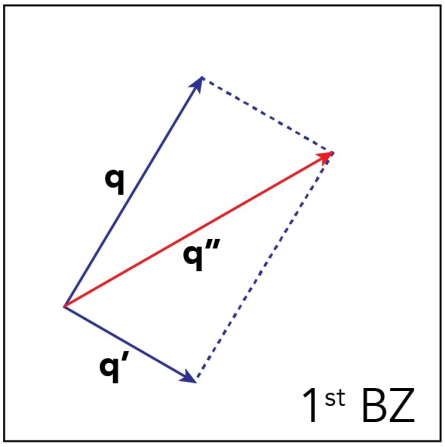

Figure 2.5: N-process

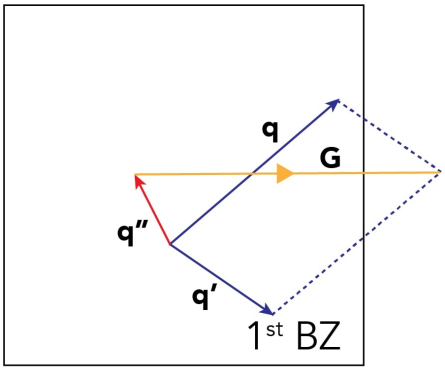

Figure 2.6: U-process

$$\mathbf{k} + \mathbf{k}' = \mathbf{k}'' + \mathbf{G} \tag{2.20}$$

The annihilation of one phonon can be described by the following energy and momentum conservation as:

$$w(\mathbf{k}, j) = w(\mathbf{k}', j') + w(\mathbf{k}'', j'') \tag{2.21}$$

$$\mathbf{k} + \mathbf{G} = \mathbf{k}' + \mathbf{k}'' \tag{2.22}$$

If **G=0**, then the process is called three-phonon normal process (N-process) (see Fig.(2.5)), otherwise, the process is called Umklapp process (U-process) (see Fig.(2.6)). The Umklapp process creates a resistance to the heat flow of phonons, while normal process enhances the heat flow. This is because N-processes have the resulting states within the first Brillouin zone after scattering, however, the U-processes have the resulting states out of the first Brillouin zone, that are reversed into first Brillouin zone using the reciprocal lattice vector **G**.
Now, we bring into play Fermi's golden rule to calculate the transition probabilities corresponding to the previously explained three phonon processes. This can be ex-

pressed as:

$$P_i^f(3ph) = \frac{2\pi}{\hbar}| < f|H^{(3)}|i > |^2\delta(E_f - E_i) \tag{2.23}$$

where i and f represent the initial and the final states respectively with E_f and E_i their corresponding energies.

For the case where two phonons annihilate, the scattering rate is:

$$P^{j'',\mathbf{k}''}_{j\mathbf{k},j'\mathbf{k}'} = \frac{2\pi}{\hbar}| < N_{j\mathbf{k}} - 1, N_{j'\mathbf{k}'} - 1, N_{j''\mathbf{k}''} + 1|H^{(3)}|N_{j\mathbf{k}}, N_{j'\mathbf{k}'}, N_{j''\mathbf{k}''} > | \tag{2.24}$$

Substituting Eq.(2.18), in the previous equation we get:

$$P^{j'',\mathbf{k}''}_{j\mathbf{k},j'\mathbf{k}'} = \frac{2\pi}{\hbar}\frac{1}{3!}\sum_{\boldsymbol{kk'k''}}\sum_{jj'j''}\delta_{G,\boldsymbol{k}+\boldsymbol{k'}+\boldsymbol{k''}}V^{(3)}(\boldsymbol{kj, k'j', k''j''}) \tag{2.25}$$

$$| < N_{j\mathbf{k}}-1, N_{j'\mathbf{k}'}-1, N_{j''\mathbf{k}''}+1|(a^+_{\mathbf{k}j}-a^-_{\mathbf{k}j})(a^+_{\mathbf{k}'j'}-a^-_{\mathbf{k}'j'})(a^+_{\mathbf{k}''j''}-a^-_{\mathbf{k}''j''})|N_{j\mathbf{k}}, N_{j'\mathbf{k}'}, N_{j''\mathbf{k}''} > |$$

The only remaining term is $a^-_{\mathbf{k}j}a^-_{\mathbf{k}'j'}a^+_{\mathbf{k}''j''}$, thus, $P^{j'',\mathbf{k}''}_{j\mathbf{k},j'\mathbf{k}'}$ becomes:

$$\begin{aligned} P^{j''\mathbf{k}''}_{j\mathbf{k},j'\mathbf{k}'} = 2\pi|V^{(3)}(\boldsymbol{-kj, -k'j', k''j''})|^2 N_{j\mathbf{k}}N_{j'\mathbf{k}'}(N_{j''\mathbf{k}''}+1) \\ \times\delta(w(\mathbf{k},j) + w(\mathbf{k}',j') - w(\mathbf{k}'',j'')) \end{aligned} \tag{2.26}$$

Similarly, the transition probability for the one phonon annihilation is :

$$\begin{aligned} P^{j'\mathbf{k}',j''\mathbf{k}''}_{j\mathbf{k}} = 2\pi|V^{(3)}(\boldsymbol{-kj, k'j', k''j''})|^2 N_{j\mathbf{k}}(N_{j'\mathbf{k}'}+1)(N_{j''\mathbf{k}''}+1) \\ \times\delta(w(\mathbf{k},j) - w(\mathbf{k}',j') - w(\mathbf{k}'',j'')) \end{aligned} \tag{2.27}$$

The total rate of change is given as the difference between forward and backward scattering as:

$$P^{j''\mathbf{k}''}_{j\mathbf{k},j'\mathbf{k}'} - P^{j\mathbf{k},j'\mathbf{k}'}_{j''\mathbf{k}''} = 2\pi\delta(w(\mathbf{k},j) + w(\mathbf{k}',j') - w(\mathbf{k}'',j''))|V^{(3)}(\boldsymbol{-kj, -k'j', k''j''})|^2 \tag{2.28}$$
$$[N_{j\mathbf{k}}N_{j'\mathbf{k}'}(N_{j''\mathbf{k}''}+1) - (N_{j\mathbf{k}}+1)(N_{j'\mathbf{k}'}+1)(N_{j''\mathbf{k}''})]$$

$$P^{j'\mathbf{k}',j''\mathbf{k}''}_{j\mathbf{k}} - P^{j\mathbf{k}}_{j''\mathbf{k}'',j'\mathbf{k}'} = 2\pi\delta(w(\mathbf{k},j) - w(\mathbf{k}',j') - w(\mathbf{k}'',j''))|V^{(3)}(\boldsymbol{-kj, k'j', k''j''})|^2 \tag{2.29}$$
$$[N_{j\mathbf{k}}(N_{j'\mathbf{k}'}+1)(N_{j''\mathbf{k}''}+1) - (N_{j\mathbf{k}}+1)(N_{j'\mathbf{k}'})(N_{j''\mathbf{k}''})]$$

Now, we can write the perturbed phonon distribution as an expansion around equilibrium using first order perturbation $\psi_{j\mathbf{k}}$:

$$N_{j\mathbf{k}} \approx \bar{N}_{j\mathbf{k}} - \frac{\partial\bar{N}_{j\mathbf{k}}}{\partial w(j\mathbf{k})}\psi_{j\mathbf{k}} \tag{2.30}$$

which gives,

$$N_{j\mathbf{k}} = \bar{N}_{j\mathbf{k}} + \bar{N}_{j\mathbf{k}}(\bar{N}_{j\mathbf{k}} + 1)\psi_{j\mathbf{k}} \tag{2.31}$$

where, $\bar{N}_{j\mathbf{k}} = \frac{1}{exp(\frac{\hbar w(j\mathbf{k})}{k_b T})-1}$ is the equilibrium phonon distribution.

By substituting Eq.(2.31) in Eq.(2.28) and linearizing it, we get:

$$P^{j''\mathbf{k}''}_{j\mathbf{k},j'\mathbf{k}'} - P^{j\mathbf{k},j'\mathbf{k}'}_{j''\mathbf{k}''} = \tilde{P}^{j''\mathbf{k}''}_{j\mathbf{k},j'\mathbf{k}'}(\psi_{j\mathbf{k}} + \psi_{j'\mathbf{k}'} - \psi_{j''\mathbf{k}''}) \tag{2.32}$$

where,

$$\begin{aligned}\tilde{P}^{j''\mathbf{k}''}_{j\mathbf{k},j'\mathbf{k}'}, = 2\pi|V^{(3)}(\boldsymbol{-kj, -k'j', k''j''})|^2 \bar{N}_{j\mathbf{k}}\bar{N}_{j'\mathbf{k}'}(\bar{N}_{j''\mathbf{k}''} + 1) \\ \times\delta(w(\mathbf{k}, j) + w(\mathbf{k}', j') - w(\mathbf{k}'', j''))\end{aligned} \tag{2.33}$$

Similarly,

$$P^{j'\mathbf{k}',j''\mathbf{k}''}_{j\mathbf{k}} - P^{j\mathbf{k}}_{j''\mathbf{k}'',j'\mathbf{k}'} = \tilde{P}^{j'\mathbf{k}',j''\mathbf{k}''}_{j\mathbf{k}}(\psi_{j\mathbf{k}} - \psi_{j'\mathbf{k}'} - \psi_{j''\mathbf{k}''}) \tag{2.34}$$

where,

$$\times\delta(w(\mathbf{k}, j) - w(\mathbf{k}', j') - w(\mathbf{k}'', j'')) \tag{2.35}$$

The final scattering rate including both processes is given by their sum:

$$-\frac{\partial N_{j\mathbf{k}}}{\partial t}|_{scatt} = \sum_{j'\mathbf{k}'j''\mathbf{k}''} [(P^{j''\mathbf{k}''}_{j\mathbf{k},j'\mathbf{k}'} - P^{j\mathbf{k},j'\mathbf{k}'}_{j''\mathbf{k}''}) + \frac{1}{2}(P^{j'\mathbf{k}',j''\mathbf{k}''}_{j\mathbf{k}} - P^{j\mathbf{k}}_{j''\mathbf{k}'',j'\mathbf{k}'})] \tag{2.36}$$

$$\begin{aligned}= \sum_{j'\mathbf{k}'j''\mathbf{k}''} \tilde{P}^{j''\mathbf{k}''}_{j\mathbf{k},j'\mathbf{k}'}(\psi_{j\mathbf{k}} + \psi_{j'\mathbf{k}'} - \psi_{j''\mathbf{k}''}) \\ + \frac{1}{2}\tilde{P}^{j'\mathbf{k}',j''\mathbf{k}''}_{j\mathbf{k}}(\psi_{j\mathbf{k}} - \psi_{j'\mathbf{k}'} - \psi_{j''\mathbf{k}''})\end{aligned}$$

To ensure that no identical processes are double counted, each term is considered. The first term corresponds to two phonons being destroyed and one created, and the second term corresponds to one phonon creating two phonons.

Now, equating with Eq.(2.7) we get:

$$\begin{aligned}\mathbf{v}_k.\boldsymbol{\nabla}T\frac{\partial N_{kj}(k)}{\partial T} = \sum_{j'\mathbf{k}'j''\mathbf{k}''} \tilde{P}^{j''\mathbf{k}''}_{j\mathbf{k},j'\mathbf{k}'}(\psi_{j\mathbf{k}} + \psi_{j'\mathbf{k}'} - \psi_{j''\mathbf{k}''}) \\ + \frac{1}{2}\tilde{P}^{j'\mathbf{k}',j''\mathbf{k}''}_{j\mathbf{k}}(\psi_{j\mathbf{k}} - \psi_{j'\mathbf{k}'} - \psi_{j''\mathbf{k}''})\end{aligned} \tag{2.37}$$

2.2.4 Relaxation Time Approximation (RTA)

According to the relaxation time approximation (RTA), the scattering rate of a given phonon mode is independent of the other phonon mode perturbations. Then, Eq.(2.36) becomes:

$$\begin{aligned}-\frac{\partial N_{j\mathbf{k}}}{\partial t}|_{scatt} = \pi\psi_{j\mathbf{k}}\bar{N}_{j\mathbf{k}}(\bar{N}_{j\mathbf{k}}+1)\sum_{j'\mathbf{k}',j''\mathbf{k}''}|V^{(3)}(-\boldsymbol{kj},\boldsymbol{k'j'},\boldsymbol{k''j''})|^2 \\ \times[2(\bar{N}_{j'\mathbf{k}'}-\bar{N}_{j''\mathbf{k}''})\delta(w(\mathbf{k},j)+w(\mathbf{k}',j')-w(\mathbf{k}'',j'')) \\ -(1+\bar{N}_{j'\mathbf{k}'}+\bar{N}_{j''\mathbf{k}''})\delta(w(\mathbf{k},j)-w(\mathbf{k}',j')-w(\mathbf{k}'',j''))]\end{aligned} \tag{2.38}$$

On the other hand, using relaxation time approximation the left term can be written as:

$$-\frac{\partial N_{j\mathbf{k}}}{\partial t}|_{scatt} = \frac{\bar{N}_{j\mathbf{k}}(\bar{N}_{j\mathbf{k}}+1)}{\tau_{j\mathbf{k}}} = \frac{N_{j\mathbf{k}}-\bar{N}_{j\mathbf{k}}}{\tau_{j\mathbf{k}}} \tag{2.39}$$

Equating Eq.(2.38) and Eq.(2.39),

$$\begin{aligned}\frac{1}{\tau^{anh}_{j\mathbf{k}}} = \sum_{j'\mathbf{k}',j''\mathbf{k}''}|V^{(3)}(-\boldsymbol{kj},\boldsymbol{k'j'},\boldsymbol{k''j''})|^2[2(\bar{N}_{j'\mathbf{k}'}-\bar{N}_{j''\mathbf{k}''})\delta(w(\mathbf{k},j)+w(\mathbf{k}',j')-w(\mathbf{k}'',j'')) \\ -(1+\bar{N}_{j'\mathbf{k}'}+\bar{N}_{j''\mathbf{k}''})\delta(w(\mathbf{k},j)-w(\mathbf{k}',j')-w(\mathbf{k}'',j''))]\end{aligned} \tag{2.40}$$

Four phonon scattering

The interactions between four phonons can take place at high temperature, since the interaction between phonons becomes more probable. By following the procedure described above, using the quartic anharmonicity the relaxation time associated with four-phonon processes can be calculated.
The transition probabilities corresponding to the four phonon processes can thus be written as:

$$\begin{aligned}P^f_i(4ph) = \frac{2\pi}{\hbar}(|<f|H^{(4)}|i>|^2 + |\sum_{m\neq i,f}\frac{<f|H^{(3)}|m><m|H^{(3)}|i>}{E_i-E_m}|^2) \\ \times\delta(E_f-E_i)\end{aligned} \tag{2.41}$$

where, m is the energy of an intermediate virtual phonon state.

Following the same procedure of the derivation discussed above, the relaxation time associated with four-phonon single-mode is:

$$\frac{1}{\tau_{\mathbf{k}j}} = \frac{1}{\bar{N}_{j\mathbf{k}}(\bar{N}_{j\mathbf{k}}+1)}\sum_{j'\mathbf{k}'j''\mathbf{k}''j'''\mathbf{k}'''}\frac{1}{2}P^{j''\mathbf{k}'',j'''\mathbf{k}'''}_{j\mathbf{k},j'\mathbf{k}'} + \frac{1}{3!}P^{j'\mathbf{k}',j''\mathbf{k}'',j'''\mathbf{k}'''}_{j\mathbf{k}} \tag{2.42}$$

where the factors 1/2 and 1/3! are to compensate for over counting of equivalent terms.

Phonon-isotope scattering

The major contribution to the relaxation time comes from the phonon-phonon scattering, which was calculated above. However, there is a significant contribution that is due to the imperfections present in the real material like isotopes, grain boundary, vacancies, dislocations etc.

Suppose $\bar{M}$ is the average mass of the solid under study. Thus, we can write:

$$\bar{M} = \sum_i f_i M_i = \frac{1}{N_r} \sum_{lk} M_{lk} \tag{2.43}$$

The fraction of unit cells having mass M_i is represented as f_i. Then, the Hamiltonian of the crystal can be written as:

$$H = H_0 + H_I \tag{2.44}$$

where H_0 is the unperturbed Hamiltonian in the harmonic approximation Eq.(3.5). Furthermore, H_I is defined as:

$$H_I = \sum_{lk\alpha} \frac{1}{2}(M_k - \bar{M})\dot{u}_\alpha^2(lk) = \sum_{lk\alpha} \frac{1}{2}(\Delta M_k)\dot{u}_\alpha^2(lk) \tag{2.45}$$

such that ΔM_k represents the perturbation at the atomic site (lk). As mentioned before, by introducing raising and lowering operators (a full mathematical proof is found in reference [39]), with u_α being:

$$\textbf{u (lk)} = -i \sum_{j\mathbf{k}} \sqrt{\frac{\hbar}{2\bar{M} N_r w(j\mathbf{k})}} e(\mathbf{l}|j\mathbf{k})[a_{j\mathbf{k}}^+ - a_{j\mathbf{k}}^-] exp(i\mathbf{k}(\mathbf{x}(l)) \tag{2.46}$$

Substituting it in the perturbed Hamiltonian gives:

$$\begin{aligned} H_I = \frac{\hbar}{4} \sum_{l\mathbf{k}\mathbf{k'}} \sum_{jj'} \sum_l \sqrt{w(j\mathbf{k})w(j'\mathbf{k'})} \frac{\Delta M_k(lk)}{N_r \bar{M}(l)} \\ e(\mathbf{l}|j\mathbf{k}) e(\mathbf{l}|j'\mathbf{k'})[a_{j\mathbf{k}}^- a_{j'\mathbf{k'}}^+ + a_{j\mathbf{k}}^+ a_{j'\mathbf{k'}}^-] exp(i\mathbf{k}(\mathbf{x}(l) + \mathbf{x}(l')) \end{aligned} \tag{2.47}$$

Using Fermi's golden rule, the transition scattering rate for the isotope scattering, similar to the three phonon interaction, can be written as:

$$P_i^f = \frac{2\pi}{\hbar} | < f|H_I|i > |^2 \delta(E_f - E_i) \tag{2.48}$$

The net scattering rate for a phonon mode is then given as:

$$-\frac{\partial N_{j\mathbf{k}}}{\partial t}|_{scatt} = \sum_{j'\mathbf{k'}} P_{j\mathbf{k}}^{j'\mathbf{k'}} - P_{j'\mathbf{k'}}^{j\mathbf{k}} \tag{2.49}$$

Following the same mathematical steps as done for three phonon-scattering, we find that the relaxation time associated with mass-difference is:

$$\frac{1}{\tau^{iso}_{\mathbf{k}j}} = \frac{\pi}{2} w^2(j\mathbf{k}) \sum_{j'\mathbf{k'}} |\sum_{l\mathbf{Q}} \Delta M(\mathbf{Q}) e(\mathbf{l}|j\mathbf{k}) e^*(\mathbf{l}|j'\mathbf{k}') \delta(\boldsymbol{q} - \boldsymbol{q'} + \boldsymbol{Q})|^2 \delta(w - w(j\mathbf{k})) \tag{2.50}$$

where $\Delta M(\mathbf{Q})$ is the Fourier transform of $\Delta M(\mathbf{lk})$ defined as:

$$\Delta M(\mathbf{Q}) = \frac{1}{N_r} \sum \Delta M(\mathbf{lk}) exp(-i\mathbf{Q}l) \tag{2.51}$$

Eventually, according to Matthiessens rule[40], the total relaxation time is given as:

$$\frac{1}{\tau_{\mathbf{k}j}} = \frac{1}{\tau^{anh}_{\mathbf{k}j}} + \frac{1}{\tau^{iso}_{\mathbf{k}j}} \tag{2.52}$$

To make the values more reliable. boundary scattering has to be accounted for. For that reason, we used an analytically derived model that will be discussed thoroughly in chapter 4.

Calculation of Thermal properties using RTA

Thermal conductivity can be calculated from the Boltzmann transport equation with the aid of RTA, as stated before :

$$\mathbf{v}_k . \boldsymbol{\nabla} T \frac{\partial N_{kj}(k)}{\partial T} = -\frac{N_{j\mathbf{k}} - \bar{N}_{j\mathbf{k}}}{\tau_{j\mathbf{k}}} \tag{2.53}$$

We have considered that the temperature gradient is very weak to change the equilibrium distribution of phonons, thus,

$$\mathbf{v}_k . \boldsymbol{\nabla} T \frac{\partial \bar{N}_{kj}(k)}{\partial T} = -\frac{N_{j\mathbf{k}} - \bar{N}_{j\mathbf{k}}}{\tau_{j\mathbf{k}}} \tag{2.54}$$

Then,

$$N_{j\mathbf{k}} = \bar{N}_{j\mathbf{k}} - \tau_{j\mathbf{k}} (\mathbf{v}_{jk} . \boldsymbol{\nabla} T \frac{\partial \bar{N}_{kj}(k)}{\partial T}) \tag{2.55}$$

A phonon with mode j**k** and an energy $\hbar w_{j\mathbf{k}}$ cause a heat current that can be written as:

$$J_{j\mathbf{k}} = \hbar w_{j\mathbf{k}} \mathbf{v}_{j\mathbf{k}} \tag{2.56}$$

Integrating Eq.(2.56) over all the phonon modes resides:

$$J = \frac{1}{8\pi^3} \sum_j \int \hbar w_{j\mathbf{k}} \mathbf{v}_{j\mathbf{k}} N_{j\mathbf{k}} d\mathbf{k} \tag{2.57}$$

The equilibrium distribution is isotropic, hence, $\sum_j \int \hbar w_{j\mathbf{k}} \bar{N}_{j\mathbf{k}} d\mathbf{k} = 0$. Now, if we substitute Eq.(2.55) in Eq.(2.57) we get:

$$J = -\frac{1}{8\pi^3} \sum_j \int \hbar w_{j\mathbf{k}} \mathbf{v}_{j\mathbf{k}} \tau_{j\mathbf{k}} (\mathbf{v}_{jk}.\boldsymbol{\nabla} T \frac{\partial \bar{N}_{kj}(k)}{\partial T}) d\mathbf{k} \tag{2.58}$$

$$= -(\frac{1}{8\pi^3} \sum_j \int \mathbf{v}_{j\mathbf{k}} \mathbf{v}_{jk} \tau_{j\mathbf{k}} C_v d\mathbf{k}) \boldsymbol{\nabla} T \tag{2.59}$$

The lattice thermal conductivity is given by Fourier's law as:

$$J = -k_l \nabla T \tag{2.60}$$

k_l is the proportionality constant.

By comparison, thermal conductivity can we written as:

$$k_l = \frac{1}{8\pi^3} \sum_j \int {\mathbf{v}_{jk}}^2 \tau_{j\mathbf{k}} C_v d\mathbf{k} \tag{2.61}$$

with C_v being the heat capacity at constant volume and τ calculated as prescribed above.

$$C_v = k_B (\frac{\hbar w_{j\mathbf{k}}}{k_B T})^2 \bar{N}_{j\mathbf{k}} (\bar{N}_{j\mathbf{k}} + 1) \tag{2.62}$$

2.2.5 Limitations of BTE-RTA

In RTA, both the N and U processes are treated as being purely resistive. Therefore, unlike the iterative solution, RTA tends to underestimate the lattice thermal conductivity k_l . Though, the differences between RTA and iterative BTE results are less significant for the materials where U-processes are more dominant as for Si (see Fig.(2.1) and Ge Fig.(2.2)). Moreover, in the relaxation-time approximation, it is assumed that the probability of scattering is independent of the phonon distribution before and after a collision, which is almost untrue.

2.2.6 Iterative Method

The iterative solution to the linearized phonon BTE is a theoretical framework in which the thermal properties can be calculated without adjustable parameters, through which it utilizes the IFCs obtained from ab-initio methods[41].

The first step is writing $\psi_{j\mathbf{k}}$ in Eq.(2.36) in terms of a function f_{jk} defined as follows:

$$\psi_{j\mathbf{k}} = -\sum_\alpha f_{j\mathbf{k}\alpha} \frac{\partial T}{\partial x_\alpha} \tag{2.63}$$

Now, substituting Eq.(2.63) in Eq.(2.36), we get:

$$Q_{j\mathbf{k}} f_{j\mathbf{k}\alpha} = k_B T v_{j\mathbf{k}\alpha} \frac{\partial \bar{N}_{j\mathbf{k}}}{\partial T} + \sum_{j'\mathbf{k}'j''\mathbf{k}''} \tilde{P}^{j''\mathbf{k}''}_{j\mathbf{k},j'\mathbf{k}'} (f_{j''\mathbf{k}''\alpha} - f_{j'\mathbf{k}'\alpha}) + \frac{1}{2} \tilde{P}^{j'\mathbf{k}',j''\mathbf{k}''}_{j\mathbf{k}} (f_{j''\mathbf{k}''\alpha} + f_{j'\mathbf{k}'}\alpha) \tag{2.64}$$

where

$$Q_{j\mathbf{k}} = \sum_{j'\mathbf{k}'j''\mathbf{k}''} (\tilde{P}^{j''\mathbf{k}''}_{j\mathbf{k},j'\mathbf{k}'} + \frac{1}{2} \tilde{P}^{j'\mathbf{k}',j''\mathbf{k}''}_{j\mathbf{k}}) \tag{2.65}$$

Then, evaluating the differential of the equilibrium phonon distribution, $\frac{\partial \bar{N}_{j\mathbf{k}}}{\partial T}$ we get:

$$f_{j\mathbf{k}\alpha} = f^0_{j\mathbf{k}\alpha} + \frac{1}{Q_{j\mathbf{k}}} \sum_{j'\mathbf{k}'j''\mathbf{k}''} \tilde{P}^{j''\mathbf{k}''}_{j\mathbf{k},j'\mathbf{k}'} (f_{j''\mathbf{k}''\alpha} - f_{j'\mathbf{k}'\alpha}) + \frac{1}{2} \tilde{P}^{j'\mathbf{k}',j''\mathbf{k}''}_{j\mathbf{k}} (f_{j''\mathbf{k}''\alpha} + f_{j'\mathbf{k}'\alpha}) \tag{2.66}$$

such that

$$f^0_{j\mathbf{k}\alpha} = \frac{\hbar w_{j\mathbf{k}} v_{j\mathbf{k}\alpha} \bar{N}_{j\mathbf{k}} (\bar{N}_{j\mathbf{k}} + 1)}{Q_{j\mathbf{k}}}. \tag{2.67}$$

Although the main contribution of the thermal conductivity is from phonon-phonon scattering, we have to take into account the isotopic impurity scattering which has a significant contribution especially in real materials like dislocations, grain boundaries etc. Consequently, Eq.(2.66) should be modified to include these extrinsic processes.

2.2.7 Isotopic impurity scattering

From Eq.(2.48) and following what was discussed in section 2.3, the additional contribution of impurities is:

$$P^{j'\mathbf{k}'}_{j\mathbf{k}} = \sum_{j'\mathbf{k}'} \tilde{P}^{j'\mathbf{k}'}_{j\mathbf{k}} (\psi_{j'\mathbf{k}'} - \psi_{j,\mathbf{k}}) \tag{2.68}$$

The scattering rate for phonon-impurity processes can be added to the linearized BTE in a straight forward manner as:

$$f_{j\mathbf{k}\alpha} = f^0_{j\mathbf{k}\alpha} + \frac{1}{Q_{j\mathbf{k}}} [\sum_{j'\mathbf{k}'j''\mathbf{k}''} \tilde{P}^{j''\mathbf{k}''}_{j\mathbf{k},j'\mathbf{k}'} (f_{j''\mathbf{k}''\alpha} - f_{j'\mathbf{k}'\alpha}) + \frac{1}{2} \tilde{P}^{j'\mathbf{k}',j''\mathbf{k}''}_{j\mathbf{k}} (f_{j''\mathbf{k}''\alpha} + f_{j'\mathbf{k}'\alpha}) + \sum_{j'\mathbf{k}'} \tilde{P}^{j'\mathbf{k}'}_{j\mathbf{k}} f_{j',\mathbf{k}'}] \tag{2.69}$$

but, Q_{jk} is modified now:

$$Q_{j\mathbf{k}} = \sum_{j'\mathbf{k}'j''\mathbf{k}''} (\tilde{P}^{j''\mathbf{k}''}_{j\mathbf{k},j'\mathbf{k}'} + \frac{1}{2} \tilde{P}^{j'\mathbf{k}',j''\mathbf{k}''}_{j\mathbf{k}}) + \sum_{j'\mathbf{k}'} \tilde{P}^{j'\mathbf{k}'}_{j\mathbf{k}} \tag{2.70}$$

Now, it becomes reasonable to perform direct comparisons with experimental measurements.

2.2.8 Limitations of BTE-Iterative

The iterative solution to the linearized Boltzmann equation allows an explicit evaluation of the complex collision term. However, there exist complexity of the required calculations coupled with the computational demands, that is why relaxation time approximations (RTAs) have been widely used to calculate k_l.

Chapter 3

Interfacial thermal resistance

A high density of interfaces may dominate the phonon scattering rates and become the principle determinant of the thermal conductivity. Granular materials present such a high interface density. Therefore, this chapter is dedicated to the development of a method that can be implemented using an ab-initio technique to accurately describe the thermal conductivity of a granular material made up of grains of different materials.

3.1 Kapitza Resistance

A finite interfacial thermal resistance is generated at the interface after a heat flux is applied when two different materials are placed in perfect contact. In 1941, Kapitza [42] reported an experimental evidence of a temperature drop near the boundary between liquid helium ^4He and a solid when heat flows across the boundary. The temperature discontinuity was from the interface instead of the bulk helium. He found that the thermal boundary resistance decreased as the temperature increased approximately as T^{-3}. Later on, the interfacial thermal resistances was observed between different metals and liquid ^3He, and even with solid helium[43] [44] [45]. Moreover, it was shown in these experiments that the phonons slow down in the bulk near the interface. Afterwards, Reynolds and Maris [46] [47] measured the Kapitza resistance in solid-solid interfaces and suggested that the additional increase in resistance at the boundary is due to additional quantum effects. Afterwards, experiments showed that the condition of the interface is a critical factor determining the thermal boundary resistance; such that phonon scattering at perfect interfaces is less frequent than rough interfaces.

3.1.1 Assumptions:

It is important to note that in most experiments the net heat flow across the interface is many orders of magnitude smaller than the heat flow in each material (which is defined as gross heat flow[48]). Thus, the usage of the equilibrium phonon density is justified. Consequently, it is assumed that in thermal equilibrium, the number of phonons leav-

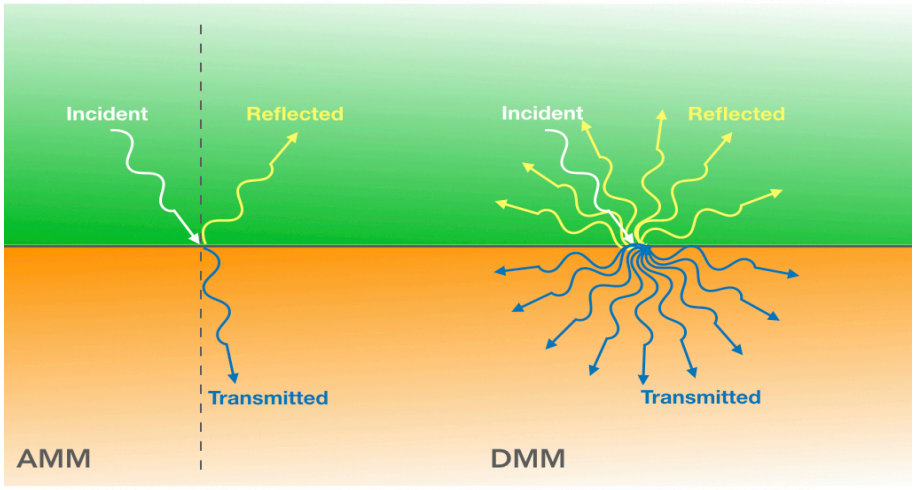

Figure 3.1: The AMM and DMM in describing phonon modes of interaction at the boundary

ing one side is the same as the number of phonons returning from the other side. This principle is known as the principle of detailed balance. Moreover, it is proposed that the materials on both sides of the interface are isotropic and the transmission probability is independent of temperature. Now, we are allowed to say that the difference between the gross heat flow from side 1 to side 2($\dot{Q}_{1\to2}(T_2)$) and the gross heat flow from side 2 to side 1($\dot{Q}_{2\to1}(T_1)$) is equal to the net heat flow from side 1 at temperature T_1 to side 2 at temperature T_2.

According to ref[50], the whole problem of finding the thermal interface conductivity reduces to computing the transmission probabilities. To do so, there exist two models for phonon transmission across an interface: the acoustic mismatch model (AMM) and the diffuse mismatch model (DMM). The first model presume that phonons either reflect or refract because they observe the interface as perfectly smooth surface. Mostly, this model works for long wavelength phonons in comparison to surface roughness [49]. On the other hand, the second model assumes that phonons see the interface as rough surface so they scatter diffusely and lose memory of their previous acoustic properties, and mostly those phonons are of short wavelength[11] Fig(3.1).

3.2 Acoustic Mismatch Model AMM

In the AMM, phonons are treated as plane waves, and the material in which the phonons propagate through is treated as continuum. Based on these assumptions, the phonon can undergo reflection. Moreover, the interface is assumed to be perfect and no scattering takes place. Hence, due to the difference of mass density and speed of sound on the two sides of the interface reflection occurs. The probabilities of each of these events are determinant by laws similar to Snell's law for light.

Consider the case where there is no polarization conversion and let θ_1 be the angle between the normal to the interface and the incident phonon wavevector. Hence, the phonon transmits with an angle θ_2 , then:

$$sin(\theta_2) = \frac{v_2(w,j)}{v_1(w,j)} sin(\theta_1) \tag{3.1}$$

where $v_1(w,j)$ and $v_2(w,j)$ are the phonon velocities in the side 1 and side 2 of the interface respectively. Herein, if the incidence angle is greater than the critical angle the probability of specular transmission is null, thus, only phonons incident with an angle smaller than the critical angle have a non-vanishing specular transmission probability and are transmitted to the other side.

Moreover, if a phonon with an incident angle θ_{in} transmits with probability α to a phonon with transmitted angle θ_{trans}, then a phonon from the other side incident on the interface with incident angle θ_{trans} transmits back into a phonon with transmitted angle θ_{in} with the same probability α that can be expressed as[50]:

$$\alpha_{1\to 2(AMM)}(w,j) = \frac{4Z_1 Z_2 cos\theta_1 cos\theta_2}{(Z_1 cos\theta_1 + Z_2 cos\theta_2)^2} \tag{3.2}$$

Here, Z is the acoustic impedance that is defined as the phonon speed multiplied by the density of the material Z_i=$\rho_i v(j,w)$. Therefore, this permits writing the probability for a phonon specular reflection at the interface as:

$$R_{1\to 2(AMM)}(w,j) = 1 - \alpha_{1\to 2(AMM)}(w,j) \tag{3.3}$$

3.3 Diffuse Mismatch Model DMM

In the DMM[48], due to the assumption of total elastic diffuse scattering, the acoustic correlations at the interface are assumed to be completely destroyed, ergo, what determines the transmission probability are the phonon densities of states of the materials in contact. Since it is assumed in the DMM that the phonon loses memory of its initial state, the transmission probability from side 1 to 2 must be 1-$\alpha_{2\to 1}$(the reflectivity

from one side must equal the transmissivity from the other). By invoking the principle of detailed balance, the number of phonons leaving side 1 equal to the number of phonons leaving side 2, per unit area per unit time. Then,

$$\sum_j v_1(w,j).N_1(w,j)\alpha_{1\to 2}(w,j) = \sum_j v_2(w,i,j).N_2(w,i,j)(1-\alpha_{1\to 2}(w,j)) \quad (3.4)$$

Then, the transmission probability can be calculated under the assumption of diffuse scattering as:

$$\alpha_{1\to 2(DMM)}(w,j) = \frac{\sum_j v_2(w,j).N_2(w,j)}{\sum_j v_1(w,j).N_1(w,j) + \sum_j v_2(w,i,j).N_2(w,i,j)} \quad (3.5)$$

Now, to calculate the thermal boundary conductance G, that is defined as the ratio of the heat current density $Q_{1\to 2}$ to the temperature differential ΔT, we use:

$$G = \frac{1}{2(2\pi)^3}\sum_{i,j}\int_k \frac{1}{k_B T^2}\alpha_{1\to 2(DMM)}(w,i,j)(\hbar w)^2|\mathbf{v}_1(w,i,j).\mathbf{n}|\frac{e^{(\frac{\hbar w}{k_B T})}}{(e^{(\frac{\hbar w}{k_B T})}-1)^2}d\mathbf{k} \quad (3.6)$$

where w and v are the phonon frequency and group velocity corresponding to wave vector k in medium 1, and n is the unit vector normal to the interface.

The major difference between these two models is that the AMM proposes a completely specular interface and the DMM assumes a completely diffuse interface. Consequently, at temperatures below 1k (low temeratures) AMM works well, because in that case the phonon wavelengths are much longer than than the interface roughness. On the contrary, the DMM works better for higher temperatures when the phonon wavelengths are comparable to the interface roughness.

In this thesis, to account for the thermal boundary conductance between layers of grains we used the DMM, because we are working at high temperatures and grain boundaries are rough. Moreover, to evaluate the integral numerically, we convert the integral over the Brillouin zone into a summation by discretizing the Brillouin zone into small volumes each of size Δk. Furthermore, we have computed the phonons frequencies $w's$ from SIESTA by computing the band structure, and we have found the velocities by deriving w with respect k.

Chapter 4

Thermal Conductivity in Si/Ge mixture of grains

The theoretical studies of the thermal conductivity of such granular materials are challenging due to the complexity of the nanostructures and the need to describe very accurately the boundary and interface effects. Molecular dynamics (MD) simulations can be used to calculate thermal conductivity for these structures directly. However, the potentials used are simplified due to computational and numerical convergence issues, hence a poor agreement with experimental results. On the other hand, density functional theory (DFT) is used to calculate the thermal conductivity directly from the Boltzmann transport equation (BTE), and shows excellent agreement with experiment, but are limited to bulk materials. Consequently, the role of alloying and nanostructuring has to be incorporated analytically through models that include scattering rates at boundaries and interfaces Fig.(4.1).

4.1 Thermal Conductivity in a Single Grain

The scattering of phonons due to temperature gradient is described by:

$$\frac{\partial N_{ks}}{\partial t}|_{scatt} = -c_s(k)\nabla T\frac{\partial N_{ks}}{\partial T} \tag{4.1}$$

where k denotes the phonon wave vector and s denotes the phonon polarization. N_{ks} is the distribution out of equilibrium of phonons of mode k and polarization s. $c_s(k)$ is the group velocity of mode k and polarization s.

In steady state regime, the total change in N_{ks} must vanish, hence:

$$\frac{\partial N_{ks}}{\partial t}|_{diff} + \frac{\partial N_{ks}}{\partial t}|_{scatt} = 0$$

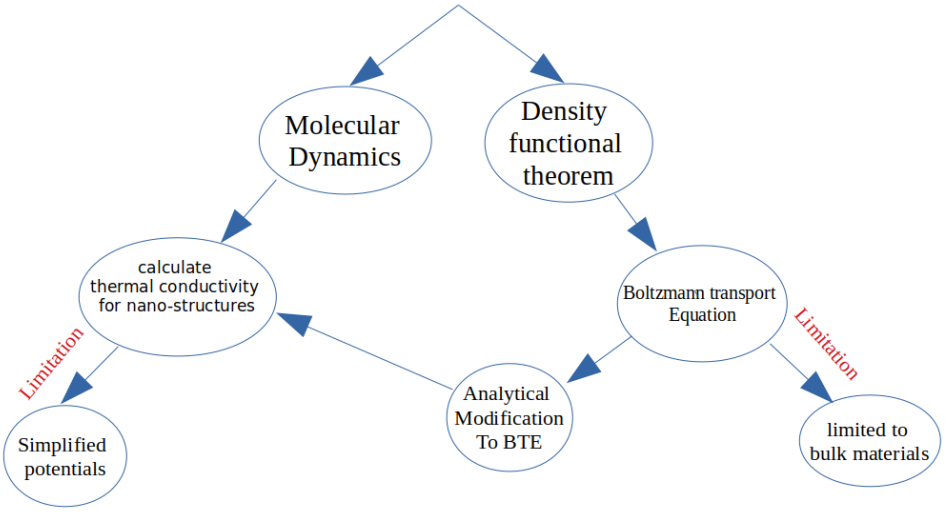

Figure 4.1: Theoretical Determination of the Thermal Conductivity

$$\frac{\partial N_{ks}}{\partial t}|_{scatt} - c_s(k)\nabla T\frac{\partial N_{ks}}{\partial T} = 0 \tag{4.2}$$

Equation(4.2) is known as the Boltzmann transport equation for phonons.

When a finite temperature gradient is applied across the solid in a steady state regime, the heat flow per unit area takes the form :

$$Q = -\boldsymbol{\kappa}\boldsymbol{\nabla}\boldsymbol{T} \tag{4.3}$$

where κ is the material's thermal conductivity.

The heat current can be found by summing over contribution from all phonon modes. It can thus be written as:

$$Q = \frac{1}{\Omega}\sum_{k,s}\hbar\omega(ks)N_{ks}c_s(k) \tag{4.4}$$

where Ω is the volume of the solid.

The out of equilibrium distribution of phonons can be seen as: N_{ks}=$\bar{N}_{ks}$ - $\tilde{N}_{ks}$. $\bar{N}_{ks}$ is the phonon distribution at equilibrium and $\tilde{N}_{ks}$ is the deviation from equilibrium. However, the phonons in equilibrium distribution do not contribute to the heat current, hence, Eq (4.4) can be written as :

$$Q = -\frac{1}{\Omega}\sum_{k,s}\hbar\omega(ks)\tilde{N}_{ks}c_s(k) \tag{4.5}$$

Now, substituting Eq(4.5) in Eq(4.3) gives an expression of κ as the following:

$$\kappa = \frac{1}{\Omega|\nabla T|^2} \sum_{k,s} \hbar\omega(ks)\tilde{N_{ks}}\boldsymbol{c_s(k)\nabla T} \tag{4.6}$$

It is clear from Eq(4.6) that in order to evaluate κ from the phonon dispersion of the material, $\tilde{N}_{ks}$ must be found.

The Boltzmann equation can be written in the form:

$$-\boldsymbol{c_s.\nabla N_{ks}(k)} + \frac{\partial N_{ks}(k)}{\partial t} = 0 \tag{4.7}$$

where, N_{ks}=$\bar{N}_{ks}$ - $\tilde{N}_{ks}$.

We consider the temperature gradient is directed in the z-direction of a Cartesian co-ordinates system, therefore,

$$-v_x\frac{\partial N_{ks}}{\partial x} - v_y\frac{\partial N_{ks}}{\partial y} - v_z\frac{\partial N_{ks}}{\partial z} + \frac{\partial N_{ks}}{\partial t} = 0 \tag{4.8}$$

and

$$v_z\frac{d\bar{N}_{ks}}{dT}\frac{\partial T}{\partial z} + v_x\frac{\partial \tilde{N}_{ks}}{\partial x} + v_y\frac{\partial \tilde{N}_{ks}}{\partial y} + \frac{\partial N_{ks}}{\partial t} = 0 \tag{4.9}$$

In Eq(4.9), we have considered that the temperature gradient is very weak to change the equilibrium distribution of phonons, thus, along z-direction we have $N_{ks} = \bar{N}_{ks}$.

We introduced a relaxation time associated with the scattering processes. This allows writing the Boltzmann transport equation in the following form:

$$v_z\frac{d\bar{N}_{ks}}{dT}\frac{\partial T}{\partial z} + v_x\frac{\partial \tilde{N}_{ks}}{\partial x} + v_y\frac{\partial \tilde{N}_{ks}}{\partial y} + \frac{\tilde{N}_{ks}}{\tau} = 0 \tag{4.10}$$

where $\tilde{N}_{ks}$= $\tilde{N}_{ks}(x, y, v_x, v_y)$.

Now, let

$$v_x\frac{\partial \tilde{N}}{\partial x} + v_y\frac{\partial \tilde{N}}{\partial y} + \frac{\tilde{N}}{\tau} = R \tag{4.11}$$

with $R = -v_z\frac{d\bar{N}}{dT}\frac{\partial T}{\partial z}$.

In the case of infinite crystal, $\tilde{N}$ is independent of x and y, so it can be written as:$\tilde{N}$=$R\tau$. In the case of finite crystal, the first and second terms in Eq (4.11) cannot be ruled out.

Now, let $\tilde{N}'$= $\tilde{N}$ - Rτ, then the Boltzmann equation becomes:

$$v_x \frac{\partial \tilde{N}'}{\partial x} + v_y \frac{\partial \tilde{N}'}{\partial y} + \frac{\tilde{N}'}{\tau} = 0 \tag{4.12}$$

so, we obtain:

$$\frac{dx}{v_x} = \frac{dy}{v_y} = -\tau \frac{d\tilde{N}'}{\tilde{N}'} \tag{4.13}$$

Eq (4.13) has two solutions :

$$\frac{x}{v_x} - \frac{y}{v_y} = cst \tag{4.14}$$

and

$$\tilde{N}' = cst * [exp(-\frac{x}{\tau v_x}) + exp(-\frac{y}{\tau v_y})] \tag{4.15}$$

A general solution in this case can be written as:

$$\tilde{N} = R\tau + cst * [exp(-\frac{x}{\tau v_x}) + exp(-\frac{y}{\tau v_y})] \tag{4.16}$$

At the boundaries, i.e, at $x \to 0$ or/and $y \to 0$, $\tilde{N} \to \sigma_z$ where σ_z is the deviation of the distribution of phonons due to their interactions with the surface phonons propagating along the z-axis.

If the phonon is away from the boundary, $\tilde{N}$ should tend toward the bulk limit, i.e, $R\tau$ which allows writing the cst in the form $\sigma_z - \frac{R\tau}{2}$= cst. Then, $\tilde{N}$ can be written as:

$$\tilde{N} = R\frac{\tau}{2}[(1-exp(-\frac{x}{\tau v_x}))+(1-exp(-\frac{y}{\tau v_y}))]+\frac{2\sigma_z}{R\tau}[exp(\frac{-x}{\tau v_x})+(exp(\frac{-y}{\tau v_y})] \tag{4.17}$$

For $\frac{2\sigma_z}{R\tau} = 1$, the boundary becomes totally reflective and $\tilde{N} \to \tilde{N}_{bulk}$ even in the presence of boundaries.
For $\frac{2\sigma_z}{R\tau} = 0$, $\tilde{N}$ at the boundary tends to zero which means that upon interaction with the boundary, $N_{ks} = \bar{N}_{ks}$. Therefore, the boundary scattering restores back the Planck's distribution to its original value. In other words, the boundary is fully resistive.

Consequently, $\frac{2\sigma_z}{R\tau}$ plays the role of a specularity factor. We replace it here by t and consider that we have a fully diffusive boundary ($\sigma_z = 0$).

The new expression of $\tilde{N}$ takes the form:

$$\tilde{N} = R\tau - R\frac{\tau}{2}[(exp(-\frac{x}{\tau v_x})) + (exp(-\frac{y}{\tau v_y}))] \tag{4.18}$$

Therefore,

$$\tilde{N} = \tilde{N}_{bulk} - \frac{\tilde{N}_{bulk}}{2}[(exp(-\frac{x}{\tau v_x})) + (exp(-\frac{y}{\tau v_y}))] \tag{4.19}$$

with $\tilde{N}_{bulk}$=$R\tau$.

Upon replacing $\tilde{N}$ in Eq (4.6) we find that : κ_{grain}=κ_{bulk} - $\Delta\kappa$, such that κ_{bulk} is the thermal conductivity of the bulk counterpart of the grain and

$$\Delta\kappa = \frac{1}{\Omega|\nabla T|^2}\sum_{k,s}\hbar\omega(ks)\tilde{N_{bulk}}\boldsymbol{v_s(k)}\boldsymbol{\nabla T}[\frac{exp(\frac{-x}{\tau v_x})+exp(\frac{-y}{\tau v_y})}{2}] \tag{4.20}$$

It follows

$$\Delta\bar{\kappa} = \frac{\iint \Delta\kappa\, dx\, dy}{\iint\, dx\, dy}$$

$$\Delta\bar{\kappa} = \frac{1}{\Omega|\nabla T|^2}\sum_{k,s}\hbar\omega(ks)\tilde{N_{bulk}}\boldsymbol{v_s(k)}\boldsymbol{\nabla T}[\frac{\frac{\tau v_x}{l_x}(1-exp(\frac{-l_x}{\tau v_x}))+\frac{\tau v_y}{l_y}(1-exp(\frac{-l_y}{\tau v_y}))}{2}] \tag{4.21}$$

where $l_x$and l_y are the dimensions of the material along x and y.

Considering that the material is isotropic in the x-y plane, Eq(4.21) can be written as:

$$\Delta\bar{\kappa} = \frac{1}{\Omega|\nabla T|^2}\sum_{k,s}\hbar\omega(ks)\tilde{N_{bulk}}\boldsymbol{v_s(k)}\boldsymbol{\nabla T}[\frac{\frac{\Lambda}{l_x}(1-exp(\frac{-l_x}{\Lambda}))+\frac{\Lambda}{l_y}(1-exp(\frac{-l_y}{\Lambda}))}{2}] \tag{4.22}$$

$$\Delta\bar{\kappa} = \sum_{k,s}\kappa_{bulk}(ks)[\frac{\frac{\Lambda}{l_x}(1-exp(\frac{-l_x}{\Lambda}))+\frac{\Lambda}{l_y}(1-exp(\frac{-l_y}{\Lambda}))}{2}] \tag{4.23}$$

4.2 Thermal Conductivity in a Single Layer of Grains

Now, suppose that the material is formed by one layer of grains of diffusive boundary. Let x be the density of the grains of material 1 and 1-x the density of the grains of material 2 in the sample.

Let Lx, Ly, and Lz be the dimensions of the sample under consideration in the x,y, and z directions.

Therefore, x=$\frac{n_1}{N}$, where n_1 is the number of grains of material 1 and N is the total number of grains in the sample. Hence, $n_1 = xN$ and $n_2 = (1-x)N$, knowing that n_2 is the number of grains of material 2 in the sample.

Let $\frac{dq_i}{dt}$ be the heat current through the i_{th} grain, hence, we can write:

$$\frac{dq_i}{dt} = -\kappa_i\int_s \boldsymbol{\nabla T ds} \tag{4.24}$$

where κ_i is the thermal conductivity of the i_{th} grain, $\boldsymbol{\nabla T}$ is the a temperature gradient and $\boldsymbol{ds}$ is an oriented surface area element. Since we have assumed a steady state regime and temperature gradient along z-axis of the grain, we can write:

$$\frac{dq_i}{dt} = -\kappa_i \nabla T.s_i \tag{4.25}$$

with s_i the cross sectional area of the i_{th} grain.

The heat current in the entire sample can thus be written as:

$$\frac{dQ_i}{dt} = -\sum_{i=1}^{N} \kappa_i \nabla T.s_i \tag{4.26}$$

If we assume an average cross sectional area $\bar{s}_i$ defined as $l_x \times l_y$, then Eq (4.26) becomes:

$$\frac{dQ_i}{dt} = -\nabla T.\bar{s}_i \sum_{i=1}^{N} \kappa_i \tag{4.27}$$

or

$$\frac{dQ_i}{dt} = -\nabla T.\bar{s}_i [\sum_{i=1}^{xN} \kappa_1 + \sum_{i=1}^{(1-x)N} \kappa_2] \tag{4.28}$$

where κ_1 is the thermal conductivity of a grain made of material 1 and κ_2 the thermal conductivity of a grain made of material 2.

Eq(4.28) can be written in a more reduced form as:

$$\frac{dQ_i}{dt} = -\nabla T.\bar{s}_i [xN\kappa_1 + (1-x)N\kappa_2] \tag{4.29}$$

Now, if we divide Eq(4.29) by the cross sectional area of the entire sample s_{total} , we find:

$$\frac{1}{s_{total}} \frac{dQ_i}{dt} \frac{1}{\nabla T} = -\frac{\bar{s}_i}{s_{total}} [xN\kappa_1 + (1-x)N\kappa_2] \tag{4.30}$$

The quantity on the right hand in Eq(4.30) is the negative of the thermal conductivity of the sample under consideration. Thus, we can write:

$$-\kappa_{layer} = -\frac{\bar{s}_i}{s_{total}} [xN\kappa_1 + (1-x)N\kappa_2] \tag{4.31}$$

Therefore,

$$\kappa_{layer} = \frac{1}{N} [xN\kappa_1 + (1-x)N\kappa_2] \tag{4.32}$$

Then, the conductivity of one layer becomes:

$$\kappa_{layer} = x\kappa_1 + (1-x)\kappa_2 \tag{4.33}$$

4.3 Thermal conductivity in a Superposition of Layers

We assume a superposition of N layers of grains, but we consider that all the layers have the same grain concentrations. The resistances in the z-direction adds up, so we can say that the overall resistance is given by:

$$R = [\sum_{i=2}^{N} R_1 + R_i + R^B_{(i-1)(i)}] \tag{4.34}$$

R_1 is the resistance of the first layer, R_i is the resistance of the i_{th} layer, and $R^B_{(i-1)(i)}$ is the resistance between the i_{th} layer and the $(i-1)_{th}$ layer.

Under the assumption that the layer have the same grains density and of identical thickness, R becomes:

$$R = NR_{layer} + (N-1)\bar{R}^B \tag{4.35}$$

where R is the resistance of the sample and R_{layer} is the resistance of an individual layer. Here, we have assumed an override boundary resistance $\bar{R}^B$ between the layers.

Eq(4.35) can be written in terms of thermal conductivity as:

$$\frac{L_z}{\kappa} = N\frac{l_z}{\kappa_{layer}} + (N-1)\bar{R}^B \tag{4.36}$$

Such that, κ is the total thermal conductivity of the sample, L_z is the thickness of the sample, and l_z is the average dimension of an individual grain in the z-direction.

N can be expressed as $\frac{L_z}{l_z}$. In the limit of $l_z <<< L_z$, the total thermal conductivity of the sample in the z-direction takes the form:

$$\kappa = \frac{\kappa_{layer}}{1 + \frac{\kappa_{layer}\bar{R}^B}{l_z}} \tag{4.37}$$

Now, in order to calculate the thermal conductivity of the sample, an expression for the boundary thermal resistance should be derived. However, to find the boundary thermal resistance, we use **DMM** (mentioned in the previous chapter).

If we consider that there are N grains in each layer, so among N^2 possibilities we have: (Number of grains of material 1)^2 possibilities to have an interaction between two grains of material 1 and (Number of grains of material 2)^2 possibilities to have an interaction between two grains of material 2. Hence, N^2 - (Number of grains of material 1)^2 - (Number of grains of material 2)^2 possibilities to have interaction between grains of different materials. Thus, if we assume that $R^B_{A\to B}$=$R^B_{B\to A}$ we can write the average boundary as:

$$\bar{R}^B = \frac{(xN)^2 R_{1\to 1} + [(x-1)N]^2 R_{2\to 2} + [N^2 - (xN)^2 - ((1-x)N)^2]\bar{R}_{1\to 2}}{N^2} \tag{4.38}$$

This can be reduced to:

$$\bar{R}^B = (x)^2 R_{1\to1} + (1-x)^2 R_{2\to2} + 2x(1-x)\bar{R}_{1\to2} \tag{4.39}$$

$R_{1\to1}$ and $R_{2\to2}$ are calculated with $\alpha = 1$ Eq.(3.5), since there is no resistance between similar grains. Also, $\bar{R}_{1\to2} = \frac{R_{1\to2}+R_{2\to1}}{2}$

4.4 Results

In the work of this thesis we have studied the thermal conductivity of a system formed by mixtures of Si and Ge nano-grains. Silicon-Germanium based systems have been of a huge interest, as they are suited for thermoelectric applications, electronic and optical devices[51][52]. Although, neither Si nor Ge is a good thermoelectric material, as their lattice thermal conductivity is very large at room temperature. The lattice thermal conductivity of Si is 150 W/mk whilst that of Ge is 63 W/mk. However, by alloy formation between the two elements, the lattice thermal conductivity can be strongly reduced to 10 W/mk [53]. Furthermore, their popularity increased because such a Si-Ge based system has low noise and low power consumption in electronic devices. Furthermore, Silicon and Germanium are cheap and widely abundant. For this reason, we opted to investigate a system formed from the combination of Si and Ge.

As previously mentioned, nanostructuring and alloying have been proposed as avenues to boost ZT and improve the thermoelectric conversion efficiency of semiconductors. Nanostrucuring first came from the introduction of superlattices. Superlattices are periodic structures of two types of crystals having small thickness (less than 50nm), and are grown using molecular beam epitaxy and metal-organic chemical vapour deposition [54]. Superlattices showed a thermal conductivity that is significantly reduced compared to a bulk crystal. The major cause of the dramatic drop in the thermal conductivity in superlattices is due to the existence of numerous interfaces that the phonons face during their propagation across the repeated layers of the superlattice. Thus, heat dissipation in superlattices is limited. Moreover, when the thickness of the layer is of the same order or less than the mean free path, size effects appear on the intrinsic thermal conductivity of the layer, consequently, the thermal conductivity decrease with layer thickness Fig.(4.2).

Si/Ge superlattices have higher thermal conductivities compared to the superlattices made of alloys due to the existence of both nanostructuring and alloying, thus, additional phonon scattering by mass defect in alloys is present in such a system (see Fig.(4.3)).

Although superlattices show a low lattice thermal conductivtiy compared to bulk materials, but they still conserve periodicity even if alloy effect is involved. Therefore, alloys shows lower thermal conductivity compared to the alloy of superlattices as

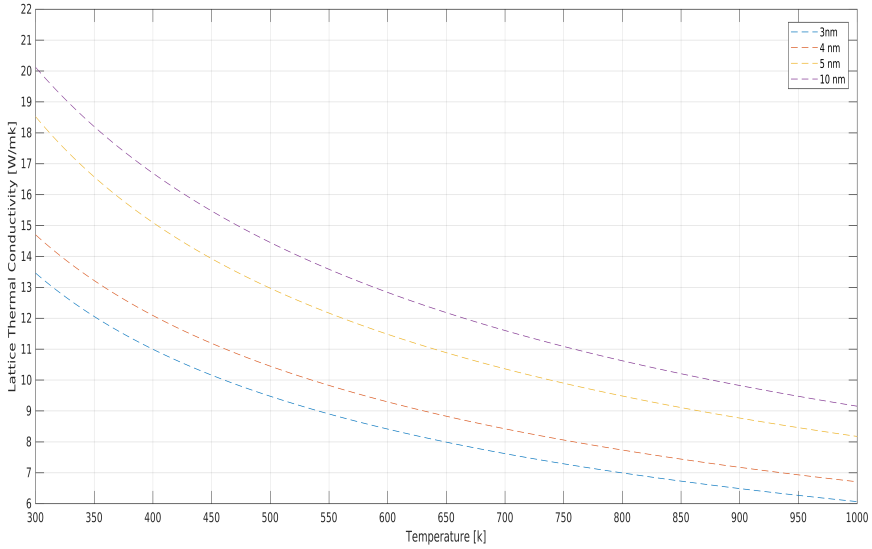

Figure 4.2: Lattice thermal conductivity of Si/Ge superlattices for different period thicknesses.

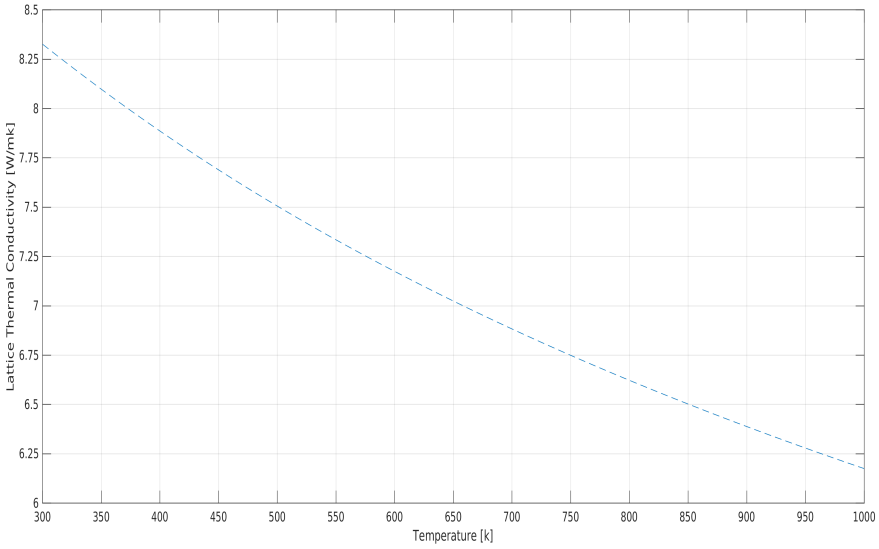

Figure 4.3: Lattice Thermal conductivity of Si/$Si_{0.7}Ge_{0.3}$ alloy of superlattice of 5 nm thickness.

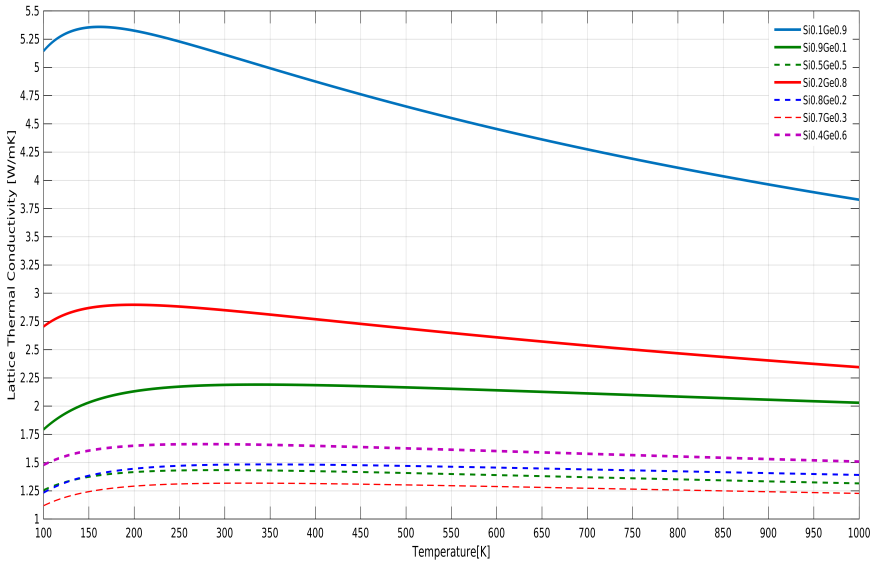

Figure 4.4: Lattice thermal conductivity of Si_xGe_{1-x} alloy for different concentrations of Si and Ge (x).

they demonstrate non-periodic systems (see Fig.(4.4)). Si-Ge alloys are very known for their high efficiency and exceptional stability at high temperatures (above 1000k) that is why they are used in NASAs radioisotope thermoelectric generators for space applications[55] [56]. To study Si-Ge alloys using DFT, the disordered crystal is replaced by ordered virtual crystal in which disorder and anharmonicity are treated as perturbations. The lattice thermal conductivity can be substantially reduced by alloy formation between the two elements. The best alloy composition in terms of thermoelectric efficiency is $Si_{0.7}Ge_{0.3}$.

However, alloys are very expensive to manufacture and sometimes desirable concentrations are unstable in nature[57] and can't be achieved. Moreover, the theoretical studies of thermal conductivity in alloys within virtual crystal approximation (VCA)[58] have their limitations due to length scales, because the bond length variations in the structure are neglected in VCA. Hence, finding a new system that can reach the alloy limit with controllable concentrations and easy to manufacture was our motivation.

In our work, based on previous sections in chapter 4, we assume that the grains are cubic with l_x=l_y=l_z. Our results showed a comparable thermal conductivity of grains with alloys of different Silicon concentrations at room temperature (see Fig.(4.5)) and at T=1175 k (see Fig.(4.6)); that is the temperature where the lowest thermal conductivity (highest ZT) is achieved for Si-Ge alloy [59]. This is because grains cause a reduction in the lattice thermal conductivity, due to phonons scattering at grain bound-

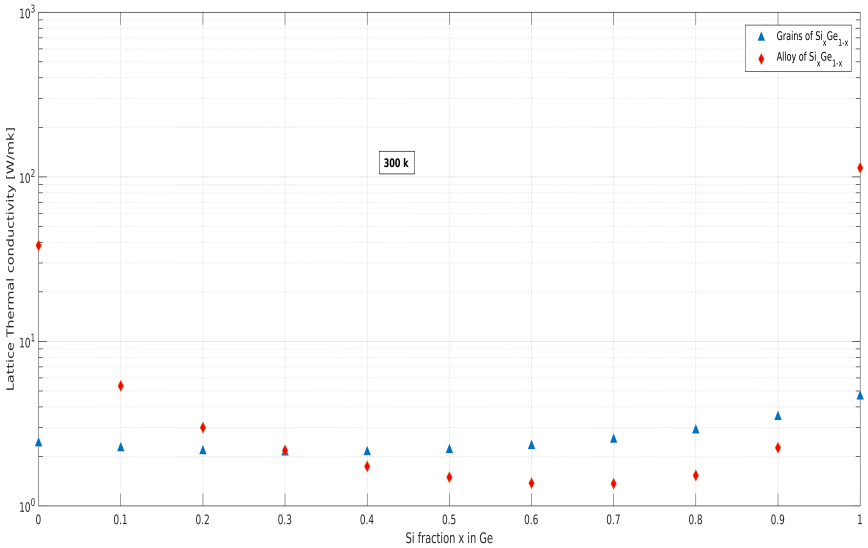

Figure 4.5: Lattice Thermal conductivity of Si_xGe_{1-x} 5 nm nano-grains compared to that of alloys for different densities x at 300 k.

aries. Furthermore, the periodicity in the proposed system is broken and hence, incoherent thermal transport will be dominant, i.e, phonons will have a probability to scatter at a high density of interfaces. We have plotted the system of grains for different sizes (see Fig.(4.7)). The boundary scattering becomes less dominant when the grain size decreases, thus, the thermal conductivity increases with the size of the grains. When the size of a single grain reached 3000 nm, we reached the bulk limit. For x=0, the thermal conductivity is 38.372 W/mk, while that of the bulk Ge it is 38.3123 W/mk. Moreover, for x=1, the conductivity is 110.3 W/mk compared to that of the bulk 113.458 W/mk. In addition, the nano-grains for pure Si(Ge) [x=1(x=0)], shows a very low thermal conductivity compared to that of the bulk Si(Ge).

4.5 Conclusion

The performance of nano-devices rely heavily on the nano scale thermal transport in their constituting materials. However, the thermal transport in nano-materials differs strongly from their bulk counterparts due to certain effects that appears upon nanostructuring such as interfaces and boundary effects. Therefore, investigating the thermal transport in such materials is of a great importance to achieve a desired high efficiency material. However, a challenge lies in investigating the thermal conductivity, since ab-initio approaches for the calculation of thermal properties exist for bulk materials

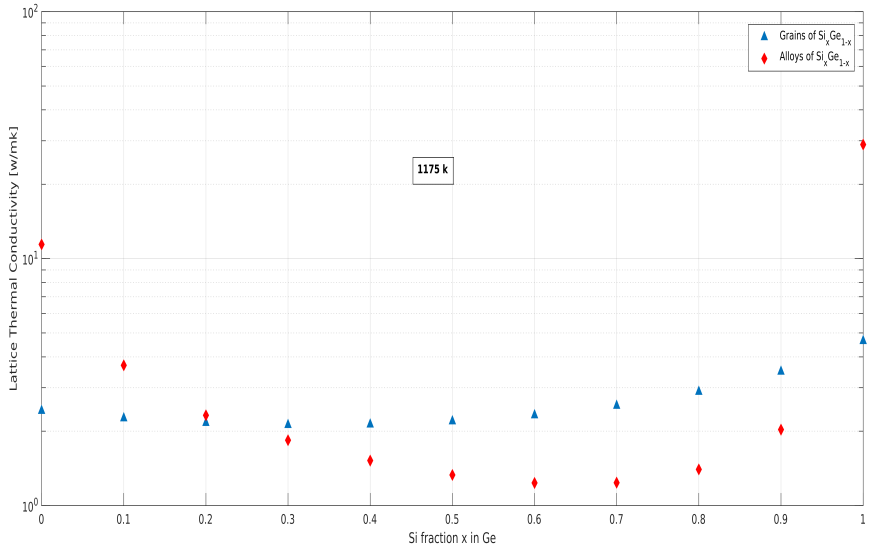

Figure 4.6: Lattice Thermal conductivity of Si_xGe_{1-x} 5 nm nano-grains compared to that of alloys for different densities x at 1175 k.

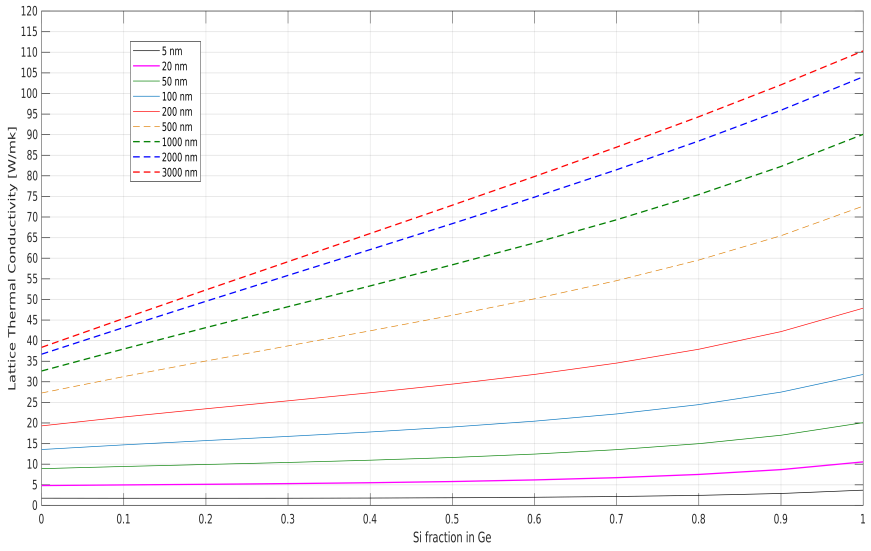

Figure 4.7: Lattice thermal conductivity of Si_xGe_{1-x} nano-grains for different grain sizes at room temperature.

but not for nano-sized materials. On the other hand, molecular dynamics simulations take into account the boundaries and interfaces, but the usage of simplified potential causes a significant deviations from experiments of up to an order of magnitude for the thermal conductivity.

In this thesis, we have developed a model to investigate the thermal transport of finite materials, and applied it to a mixture of nano-grains. This model is based on the solution of spatial dependent Boltzmann equation, and can be implemented using ab-initio techniques. The Boltzmann Transport Equation (BTE) for phonons is solved within the relaxation time approximation(RTA). In RTA, the scattering rate for a phonon mode is supposed to be independent from other phonons' perturbations modes. We could manage to calculate the thermal conductivity of finite materials by introducing correction to the thermal conductivity of the bulk counterpart, where the material size enters as a parameter. This correction relies on the calculated wave vectors and phonons mean free path, computed using AlmaBTE; an ab-initio simulation.

The interfacial resistance is accounted for by using the Diffuse mismatch model DMM. In the DMM, the interfaces between grains are assumed to be completely diffusive, with a probability of transmission that involves the exact dispersion relations of the materials at both sides. The dispersion relations are computed using ab-initio techniques for the derivation of the harmonic and anharmonic interatomic forces.

We have studied Si-Ge nano-grains due to their significant importance in thermoelectric devices. This system showed a lower thermal conductivity than bulk Si, bulk Ge, Si-Ge superlattice (with periodic interface), and superlattice of alloy. Hence, a better thermoelectric efficiency. Another key development we present in this work is that the mixture of Si-Ge nano grains showed thermal conductivity values comparable with the thermal conductivity of Si-Ge alloys. Si-Ge alloys are known by their extremely low thermal conductivity. However, most of their compositions are thermodynamically unstable. Such instability problem does not exist in the system we introduce in this work. Hence, thermoelectric systems designed theoretically with the grains mixtures we propose have a greater chance to be realized experimentally. Therefore, we hope that the work presented in this thesis opens the door for a new generation of thermoelectric devices based on grains mixtures.

Appendix A

Abbreviations

BTE	Botlzmann Transport Equation
RTA	Relaxation time approximation
MFP	Mean Free Path
AMM	Acoustic Mismatch Model
DMM	Diffuse Mismatch Model
DFT	Density Functional Theorem
LDA	Linear Density Approximation
GGA	Generalized Gradient Approximation
PBC	Periodic boundary Conditions
PP	Pseudo-Potential
BZ	Brillouin Zone
IBZ	Irreducible Brillouin Zone
KS	Kohn Sham equations
FT	Fourier Transform

Bibliography

[1] J. G. Lee, *Computational materials science: an introduction*. Crc Press, 2016.

[2] M. C. Payne, M. P. Teter, D. C. Allan, T. Arias, and a. J. Joannopoulos, "Iterative minimization techniques for ab initio total-energy calculations: molecular dynamics and conjugate gradients," *Reviews of modern physics*, vol. 64, no. 4, p. 1045, 1992.

[3] C. Glassbrenner and G. A. Slack, "Thermal conductivity of silicon and germanium from 3 k to the melting point," *Physical Review*, vol. 134, no. 4A, p. A1058, 1964.

[4] T. J. Seebeck, *Magnetische polarisation der metalle und erze durch temperaturdifferenz*. No. 70, W. Engelmann, 1895.

[5] G. J. Snyder and E. S. Toberer, "Complex thermoelectric materials," in *Materials For Sustainable Energy: A Collection of Peer-Reviewed Research and Review Articles from Nature Publishing Group*, pp. 101–110, World Scientific, 2011.

[6] L. Hicks and M. S. Dresselhaus, "Effect of quantum-well structures on the thermoelectric figure of merit," *Physical Review B*, vol. 47, no. 19, p. 12727, 1993.

[7] L. Hicks and M. S. Dresselhaus, "Thermoelectric figure of merit of a one-dimensional conductor," *Physical review B*, vol. 47, no. 24, p. 16631, 1993.

[8] J. P. Heremans, M. S. Dresselhaus, L. E. Bell, and D. T. Morelli, "When thermoelectrics reached the nanoscale," *Nature nanotechnology*, vol. 8, no. 7, p. 471, 2013.

[9] R. Venkatasubramanian, E. Silvola, T. Colpitts, and B. O'quinn, "Thin-film thermoelectric devices with high room-temperature figures of merit," in *Materials for Sustainable Energy: A Collection of Peer-Reviewed Research and Review Articles from Nature Publishing Group*, pp. 120–125, World Scientific, 2011.

[10] A. I. Hochbaum, R. Chen, R. D. Delgado, W. Liang, E. C. Garnett, M. Najarian, A. Majumdar, and P. Yang, "Enhanced thermoelectric performance of rough silicon nanowires," *Nature*, vol. 451, no. 7175, p. 163, 2008.

[11] P. Reddy, K. Castelino, and A. Majumdar, "Diffuse mismatch model of thermal boundary conductance using exact phonon dispersion," *Applied Physics Letters*, vol. 87, no. 21, p. 211908, 2005.

[12] W. Li, J. Carrete, N. A. Katcho, and N. Mingo, "Shengbte: A solver of the boltzmann transport equation for phonons," *Computer Physics Communications*, vol. 185, no. 6, pp. 1747–1758, 2014.

[13] J. M. Soler, E. Artacho, J. D. Gale, A. García, J. Junquera, P. Ordejón, and D. Sánchez-Portal, "The siesta method for ab initio order-n materials simulation," *Journal of Physics: Condensed Matter*, vol. 14, no. 11, p. 2745, 2002.

[14] W. Yang and P. W. Ayers, "Density-functional theory," in *Computational Medicinal Chemistry for Drug Discovery*, pp. 103–132, CRC Press, 2003.

[15] A. D. Becke, "A new mixing of hartree–fock and local density-functional theories," *The Journal of chemical physics*, vol. 98, no. 2, pp. 1372–1377, 1993.

[16] J. Carrete, B. Vermeersch, A. Katre, A. van Roekeghem, T. Wang, G. K. Madsen, and N. Mingo, "almabte: A solver of the space–time dependent boltzmann transport equation for phonons in structured materials," *Computer Physics Communications*, vol. 220, pp. 351–362, 2017.

[17] D. Broido, M. Malorny, G. Birner, N. Mingo, and D. Stewart, "Intrinsic lattice thermal conductivity of semiconductors from first principles," *Applied Physics Letters*, vol. 91, no. 23, p. 231922, 2007.

[18] B. Paulus and K. Rosciszewski, "Hartree–fock ground-state properties for the group 1 alkali metals and the group 11 noble metals," *Journal of Physics: Condensed Matter*, vol. 19, no. 34, p. 346217, 2007.

[19] P. Hohenberg and W. Kohn, "Inhomogeneous electron gas," *Physical review*, vol. 136, no. 3B, p. B864, 1964.

[20] W. Kohn and L. J. Sham, "Self-consistent equations including exchange and correlation effects," *Physical review*, vol. 140, no. 4A, p. A1133, 1965.

[21] J. P. Perdew and A. Zunger, "Self-interaction correction to density-functional approximations for many-electron systems," *Physical Review B*, vol. 23, no. 10, p. 5048, 1981.

[22] S. Baroni, S. De Gironcoli, A. Dal Corso, and P. Giannozzi, "Phonons and related crystal properties from density-functional perturbation theory," *Reviews of Modern Physics*, vol. 73, no. 2, p. 515, 2001.

[23] K. Lejaeghere, G. Bihlmayer, T. Björkman, P. Blaha, S. Blügel, V. Blum, D. Caliste, I. E. Castelli, S. J. Clark, A. Dal Corso, *et al.*, "Reproducibility in density functional theory calculations of solids," *Science*, vol. 351, no. 6280, p. aad3000, 2016.

[24] V. Heine and D. Weaire, "Pseudopotential theory of cohesion and structure," in *Solid state physics*, vol. 24, pp. 249–463, Elsevier, 1970.

[25] H. J. Monkhorst and J. D. Pack, "Special points for brillouin-zone integrations," *Physical Review B*, vol. 13, pp. 5188–5192, 1976.

[26] R. P. Feynman, "Forces in molecules," *Phys. Rev.*, vol. 56, pp. 340–343, Aug 1939.

[27] S. Baroni, S. de Gironcoli, A. Dal Corso, and P. Giannozzi, "Phonons and related crystal properties from density-functional perturbation theory," *Rev. Mod. Phys.*, vol. 73, pp. 515–562, Jul 2001.

[28] X. Gonze and J.-P. Vigneron, "Density-functional approach to nonlinear-response coefficients of solids," *Physical Review B*, vol. 39, no. 18, p. 13120, 1989.

[29] R. Peierls, "Zur kinetischen theorie der wärmeleitung in kristallen," *Annalen der Physik*, vol. 395, no. 8, pp. 1055–1101, 1929.

[30] J. Callaway, "Model for lattice thermal conductivity at low temperatures," *Physical Review*, vol. 113, no. 4, p. 1046, 1959.

[31] S. Volz, *Thermal nanosystems and nanomaterials*, vol. 118. Springer Science & Business Media, 2009.

[32] J. M. Haile, *Molecular dynamics simulation: elementary methods*, vol. 1. Wiley New York, 1992.

[33] S. G. Volz and G. Chen, "Molecular-dynamics simulation of thermal conductivity of silicon crystals," *Phys. Rev. B*, vol. 61, pp. 2651–2656, Jan 2000.

[34] R. Car and M. Parrinello, "Unified approach for molecular dynamics and density-functional theory," *Phys. Rev. Lett.*, vol. 55, pp. 2471–2474, Nov 1985.

[35] S. Volz, J.-B. Saulnier, M. Lallemand, B. Perrin, P. Depondt, and M. Mareschal, "Transient fourier-law deviation by molecular dynamics in solid argon," *Phys. Rev. B*, vol. 54, pp. 340–347, Jul 1996.

[36] A. Skye and P. K. Schelling, "Thermal resistivity of si–ge alloys by molecular-dynamics simulation," *Journal of Applied Physics*, vol. 103, no. 11, p. 113524, 2008.

[37] A. Ward, D. Broido, D. A. Stewart, and G. Deinzer, "Ab initio theory of the lattice thermal conductivity in diamond," *Physical Review B*, vol. 80, no. 12, p. 125203, 2009.

[38] K. Esfarjani, G. Chen, and H. T. Stokes, "Heat transport in silicon from first-principles calculations," *Physical Review B*, vol. 84, no. 8, p. 085204, 2011.

[39] M. Kazan and P. Masri, "The contribution of surfaces and interfaces to the crystal thermal conductivity," *Surface Science Reports*, vol. 69, no. 1, pp. 1 – 37, 2014.

[40] J. Bass, "Deviations from matthiessen's rule," *Advances in Physics*, vol. 21, no. 91, pp. 431–604, 1972.

[41] M. Omini and A. Sparavigna, "Beyond the isotropic-model approximation in the theory of thermal conductivity," *Physical Review B*, vol. 53, no. 14, p. 9064, 1996.

[42] E. T. Swartz and R. O. Pohl, "Thermal boundary resistance," *Rev. Mod. Phys.*, vol. 61, pp. 605–668, Jul 1989.

[43] D. Lee and H. A. Fairbank, "Heat transport in liquid he 3," *Physical Review*, vol. 116, no. 6, p. 1359, 1959.

[44] A. Anderson, J. Connolly, and J. Wheatley, "Thermal boundary resistance between solids and helium below 1 k," *Physical Review*, vol. 135, no. 4A, p. A910, 1964.

[45] R. Peterson and A. Anderson, "The kapitza thermal boundary resistance," *Journal of Low Temperature Physics*, vol. 11, no. 5-6, pp. 639–665, 1973.

[46] C. Reynolds Jr and A. Anderson, "Thermal boundary resistance to solid helium, hydrogen, deuterium, and neon," *Physical Review B*, vol. 14, no. 9, p. 4114, 1976.

[47] H. J. Maris, "Phonon transmission across interfaces and the kapitza resistance," *Physical Review B*, vol. 19, no. 3, p. 1443, 1979.

[48] E. T. Swartz and R. O. Pohl, "Thermal boundary resistance," *Reviews of modern physics*, vol. 61, no. 3, p. 605, 1989.

[49] D. G. Cahill, W. K. Ford, K. E. Goodson, G. D. Mahan, A. Majumdar, H. J. Maris, R. Merlin, and S. R. Phillpot, "Nanoscale thermal transport," *Journal of applied physics*, vol. 93, no. 2, pp. 793–818, 2003.

[50] M. Kazan, "Interpolation between the acoustic mismatch model and the diffuse mismatch model for the interface thermal conductance: Application to inn/gan superlattice," *Journal of Heat Transfer*, vol. 133, no. 11, p. 112401, 2011.

[51] G. Abstreiter, K. Eberl, E. Friess, W. Wegscheider, and R. Zachai, "Silicon/germanium strained layer superlattices," *Journal of Crystal Growth*, vol. 95, no. 1-4, pp. 431–438, 1989.

[52] G. A. Slack and M. A. Hussain, "The maximum possible conversion efficiency of silicon-germanium thermoelectric generators," *Journal of applied physics*, vol. 70, no. 5, pp. 2694–2718, 1991.

[53] C. Wood, "Materials for thermoelectric energy conversion," *Reports on progress in physics*, vol. 51, no. 4, p. 459, 1988.

[54] H. T. Grahn, *Semiconductor superlattices: growth and electronic properties*. World Scientific, 1995.

[55] A. Sanchez-Torres, "Radioisotope power systems for space applications," in *Radioisotopes* (N. Singh, ed.), ch. 21, Rijeka: IntechOpen, 2011.

[56] D. Rowe, "Applications of nuclear-powered thermoelectric generators in space," *Applied Energy*, vol. 40, no. 4, pp. 241–271, 1991.

[57] H. Baker, "Section 1 introduction to alloy phase diagrams," 1992.

[58] J. Garg, N. Bonini, B. Kozinsky, and N. Marzari, "Role of disorder and anharmonicity in the thermal conductivity of silicon-germanium alloys: A first-principles study," *Physical review letters*, vol. 106, no. 4, p. 045901, 2011.

[59] T. M. Tritt and M. Subramanian, "Thermoelectric materials, phenomena, and applications: a bird's eye view," *MRS bulletin*, vol. 31, no. 3, pp. 188–198, 2006.